The gamma model analysis:

Introducing a novel scoring method of event-related potentials

Inauguraldissertation

zur

Erlangung des Doktorgrades

der Humanwissenschaftlichen Fakultät

der Universität zu Köln

nach der Promotionsordnung vom 18.12.2018

vorgelegt von

Kilian Kummer

aus Dachau

Abgabe: August 2020

Thesis Declaration

I declare that the thesis has been composed by myself and that the work has not been submitted for any other degree or professional qualification. I confirm that the work submitted is my own, except where jointly authored publications have been included. Both my own contributions and those of the other authors to this work have been explicitly indicated below. I confirm that appropriate credit has been given within this thesis where reference has been made to the work of others.

The work presented in the abstract and in Chapters 1, 2.5, 2.6, 3.1, 3.3, 4, 5, 7, 9.2, and 9.3 is based on a previously published journal article: Kummer, K., Dummel, S., Bode, S., & Stahl, J. (2020). The gamma model analysis (GMA): Introducing a novel scoring method for the shape of components of the event-related potential. *Journal of Neuroscience Methods*, *335*, 108622.

The aforementioned journal article was slightly modified to aid reading flow; no substantial changes to the actual content were made.

This study was conceived by all of the authors. Jutta Stahl and Kilian Kummer were responsible for its conceptualisation, methodology, investigation, and writing (review & editing). Kilian Kummer carried out software and formal analysis, as well as completing the original draft. Sebastian Dummel and Stefan Bode accounted for writing (review & editing). Stefan Bode and Jutta Stahl also supervised, and Jutta Stahl was responsible for project administration.

Abstract

Research using the event-related potential (ERP) method to investigate cognitive processes has usually focused on the analysis of either individual peaks or the area under the curve as components of interest. These approaches, however, cannot analyse the substantial variation in size and shape across individual waveforms.
The aim of my thesis is thus to introduce the *gamma model analysis* (GMA). The GMA addresses these specific restrictions of the usually applied methods and enables the analysis of additional time-dependent and shape-related information on ERP components by fitting mathematically computed gamma probability density function (PDF) waveforms to an ERP.
The advantage of the GMA is demonstrated in a simulation study and a digit flanker task, as well as a force production task. The data of the digit flanker task is also used to examine a potential limitation of the GMA, namely the inability of the gamma PDF to execute a sign change. Finally, the gamma PDF was compared with three other PDFs concerning their goodness of fit.
The different gamma model parameters were sensitive to various experimental manipulations across the empirical studies. Moreover, the GMA revealed several additional interrelated but non-redundant parameters compared to the classical methods, which were predictive of different aspects of behaviour, allowing for a more nuanced analysis of the cognitive processes. The GMA provides an elegant method for extracting easily interpretable indices for the rise and decline of the components that complement the classical parameters. This approach, therefore, provides a novel toolset to better understand the exact relationship between ERP components, behaviour, and cognition.

Content

1 Introduction and Theoretical Background

One possible way to describe psychology can be as the science of perception, awareness, cognition, and behaviour. Common methods often used in psychological research include self-reports, observations, and behavioural data. Nevertheless, it also encompasses a broad range of invasive and non-invasive neuropsychological methods to investigate, for instance, cognitive functions. The electroencephalogram (EEG), especially the event-related potential (ERP), is one of these methods. ERPs are small voltage fluctuations measured by the EEG, reflecting the electrophysiological brain responses to specific (e.g. sensory, cognitive, motor) events. The first ERP component, the contingent negative variation (Walter et al., 1964), was identified approximately 30 years after the development of the EEG (Berger, 1931). Since then, the ERP has been increasingly used to gain a better understanding of electrophysiological activity in the human brain. The essential role of the ERP across various research areas has been demonstrated by the fivefold increase in research papers from 1995 to 2010 (Woodman, 2010). Since 2010, the number of published research papers has remained at a high level (Figure 1).

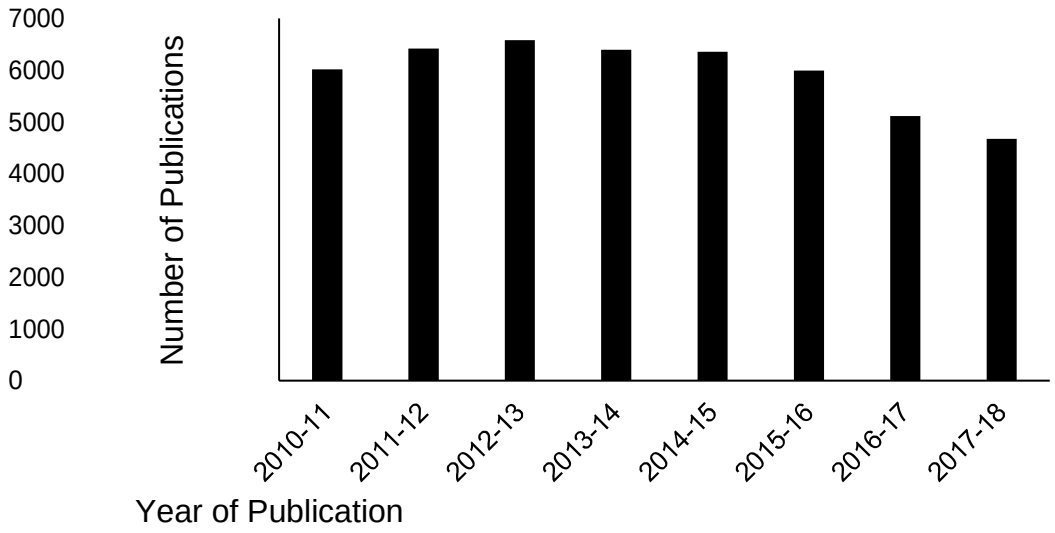

Figure 1. Number of event-related potential reports by year of publication. Data derived from PsycINFO searches for the terms event-related potential, ERP, or evoked potential in any search field (Woodman, 2010).

A vital part of the ERP research is the quantification of ERP components derived from the EEG data. Without quantification, ERP researchers could not use statistical testing, differentiate across conditions, or interpret ERP data. Two scoring methods are usually applied in the statistical analyses of ERP components: peak and area measures. The *peak amplitude* is determined by the most negative (or positive) point in a waveform within a specific time window of interest. The *area* is typically estimated by the mean activity (i.e. mean amplitude) within a specified time interval (Clayson et al., 2013). These approaches, however, cannot analyse the substantial variation in size and shape across individual waveforms (Kappenman & Luck, 2012; Luck, 2014). The aim of my thesis is thus to introduce the *gamma model analysis* (GMA): The GMA is a newly developed method which addresses these specific restrictions of the usually applied methods and enables the analysis of additional information on ERP components by fitting mathematically computed gamma waveforms to an ERP. It is therefore possible to describe the shape of the component, which was previously missed out.

The thesis starts with an overview of the biological basis of EEG and ERP. This is followed by the introduction of a well-investigated ERP component, the medial-frontal negativity (MFN), which was used to evaluate the new approach. Further, commonly applied scoring methods for the statistical analysis of ERP components and their limitations will be described, before introducing the GMA, including the gamma probability density function (PDF) and the grid restrained nelder-mead algorithm (Bűrmen et al., 2006). Forming the empirical framework of the thesis, a simulation study (Study 1; Kummer et al., 2020) to evaluate our approach will be presented. In Study 2 (Kummer et al., 2020), the reanalysed data of a digit flanker task to examine the suitability of the process of fitting our novel approach to empirical data will be described. Study 3 (Kummer et al., 2020) investigated data from a force production task which was used to identify if the GMA was sensitive to experimentally induced variations of participant force production in the MFN. The data of the digit flanker task is also used to examine a potential limitation of the GMA, namely the inability of the Gamma PDF to execute a sign change (Study 4). Finally, the Gamma PDF was compared with three other PDFs concerning their goodness of fit (Study 5). Results of all studies will then be discussed with regards to their implications to the field and possible future directions in research.

2 Biological Basis of the EEG and Event-Related Potentials

The EEG is one of the oldest and most widely used methods to investigate the electric activity within our brain (Kappenman & Luck, 2012; Luck, 2014). It takes advantage of the fact that the information processing of our brain works mainly through electrical impulses. The EEG records the electrical activity along the scalp, which is the result of a voltage fluctuation by the flow of current due to firing neurons in our brains. The EEG allows the assessment of ERP components, which are specific measurements of the brain's response to a psychologically relevant event (Bucci & Galderisis, 2011; Luck, 2014; Nisar & Kim, 2015). To understand the origins of the EEG signal and what an ERP component is, a brief introduction to the biological basis of the EEG will be given in section 2.1.

2.1 Electroencephalography

The founder of the EEG was Hans Berger, a psychiatrist with a thorough interest in the relationship between mind and body. In 1924, he invented the first non-invasive scalp EEG for humans (Berger, 1931; Boutros, 2011). The EEG records the electrical potentials generated by cerebral neurons, attenuated by meningeal layers, skull, and scalp. Electrical potentials are the electrical charge differences between two points. The two electric potentials which are important for the EEG recording are the *action potentials* and the *post-synaptic potentials* (Bucci & Galderisis, 2011; Kamel & Malik, 2015).

Before producing one of these electric potentials, a neuron has a *resting membrane potential* (-60 to -70 mV), which is generated by high concentrations of potassium (K^+) and chloride (Cl^-) ions inside a neuron, while high concentrations of sodium (Na^+) and calcium (Ca^{2+}) ions are kept outside (Birbaumer & Schmidt, 2010). Regarding the action potential, the membrane potential becomes less negative at first, because of a critical amount of Na^+ entering the cell. This process is called depolarisation. After the depolarisation, K^+ ions leave the cell and less Na^+ ions enter the cell, causing a repolarisation. The resting membrane potential can be restored.

Action potentials and thus voltage changes can pass through the cell body to axon terminals where the release of neurotransmitters (e.g. GABA, dopamine, acetylcholine) for the signal conduction is triggered, which is important for the post-synaptic potentials (Birbaumer & Schmidt, 2010; Bucci & Galderisis, 2011; Kamel & Malik, 2015). The released neurotransmitters are binding with specific receptors of a post-synaptic neuron. Through this binding, the concentration of ions across the membrane at the receptor location can change, and the consequences are post-synaptic potentials.

Post-synaptic potentials can be either depolarising or hyperpolarising. The depolarisation works, in principle, similarly to the action potentials. Thus, these post-synaptic potentials are referred to as excitatory post-synaptic potentials because they increase the likelihood of a proper action potential. In contrast to the depolarisation, a hyperpolarisation is often the result of K^+ ions leaving the cell and Cl^- ions entering the cell. These post-synaptic potentials are referred to as inhibitory post-synaptic potentials because they decrease the likelihood of an action potential. Additionally, unlike an action potential, the duration of which is about one millisecond, post-synaptic potentials can stretch up to hundreds of milliseconds (Birbaumer & Schmidt, 2010; Bucci & Galderisis, 2011; Kamel & Malik, 2015). These post-synaptic potentials are the main contributors to the neural activity measured by the EEG (Lopes da Silva, 1991). The EEG cannot detect the electrical potential produced by a single neuron, because it is too small. However, when a large group of neurons, about hundreds of thousands, show synchronised activity, the summation of the produced electrical potentials is measurable at the scalp (Luck, 2014; Nunez & Srinivasan, 2006). Thus, the EEG can record human brain activity very precisely and can simultaneously monitor hundreds of different potential processes. However, figuring out which electrical potentials in the enormous mass of recorded EEG data could be linked to neurocognitive processes remains challenging. This can at least partially be realised through ERPs, which reflect the electrophysiological brain response to specific (e.g. sensory, cognitive, motor) events (e.g. Luck, 2014).

2.2 Event-related potentials

Every psychological operation or function (e.g. action monitoring, attention mechanisms, processing of emotional stimuli) which researchers want to systematically manipulate and investigate in an experimental task (e.g. choice reaction time or force production tasks) comprises a temporal pattern of neural activity in a specific brain area (Kamel & Malik, 2015; Luck, 2014; Nisar & Kim, 2015). ERPs allow researchers to attain a deeper knowledge of the neural activity linked to the investigated psychological operations (Kropotov, 2009). The voltage change reflecting a psychological operation within a single event-locked EEG epoch is too small compared to the constantly present spontaneous neural activity. Thus, a signal processing technique is required which allows increasing the low signal-to-noise ratio. The averaging of several EEG epochs time-locked to the same repeated psychologically relevant event (e.g. stimulus, response) has proven itself to be useful in this context (Kamel & Malik, 2015; Luck, 2014; Nisar & Kim, 2015). Nevertheless, this procedure underlies two assumptions: The first assumption is that the recorded neural activity elicited through the psychological event is invariant (identical in shape and phase) throughout all trials. The second assumption is that the remaining neural background activity, recorded through the EEG, is randomly distributed noise. By averaging a sufficient number of trials, the random background activity should substantially decrease with respect to the ERP signal (Coles & Rugg, 2002; Kamel & Malik, 2015; Luck, 2014).

Luck (2014) updated the definition of the ERP from Dochin et al. (1978) as follows: “An ERP component can be operationally defined as [a] set of voltage changes that are consistent with a single neural generator site and that systematically vary in amplitude across conditions, time, individuals, and so forth” (Luck, 2014, p.68). Usually, ERP components can be identified through their polarity and their peak latency (Kappenman & Luck, 2012; Luck, 2014). The first identified ERP component was the contingent negative variation (CNV; Walter et al., 1964) The CNV shows a negative peak between 250 ms and 470 ms after a warning stimulus (Tecce, 1972). Since the early findings regarding CNV, it has become well-recognised that ERPs reflect electrophysiological brain activity. As a consequence, they became more and more important in gaining a better understanding of the human brain (Coles & Rugg, 2002; Kappenman & Luck, 2012).

A specific ERP component, the MFN (Luck, 2014), is described in the following section because this well-investigated ERP component was chosen to evaluate the GMA approach.

2.3 The medial-frontal negativity

Falkenstein et al. (1991) were the first researchers to observe a negative ERP component between 50 and 100 ms after an error had been committed by the experimental participants. They did so by analysing the response-locked waveforms of erroneous responses and correct responses in a speed choice reaction time task. This ERP component typically showed a larger negative peak-amplitude after an erroneous reaction compared to correct responses (Gehring et al., 2012).

At first, the ERP component was explained as an error-detection signal and therefore named error negativity (Ne, Falkenstein et al., 1991) or error-related negativity (Gehring et al., 1993). However, researchers later discovered a small negativity which appeared after correct responses (correct-related negativity; Gehring & Knight, 2000; Scheffers & Coles, 2000). These two ERP components seem to reflect similar mechanisms of action monitoring and are thus in combination often referred to as MFN (Armbrecht et al., 2012; Gehring & Willoughby, 2002)

The MFN does occur in speed choice reaction time tasks requiring a keypress by hand after visual stimuli (Gehring et al., 1993). Moreover, studies using tactile (Forster & Pavone, 2008) or auditory stimuli (Falkenstein et al., 1991) and oculomotor (Nieuwenhuis et al., 2001) or vocal responses (Masaki et al., 2001) elicited a MFN as well. Additionally, a sharp negative deflection does not only occur after erroneous responses, but also after partial errors: an incorrect muscular activation, which is not sufficient to produce an overt full error (Allain et al., 2004; Burle et al., 2002; Carbonnell & Falkenstein, 2006). Furthermore, the MFN also appears to be modulated by the force magnitude of a given response (peak force, PF) and the time between response onset and the peak of the produced force (time to peak, TTP; Armbrecht et al., 2012, 2013; Bruijn et al., 2003).

According to Armbrecht et al. (2013), the MFN showed a larger negative amplitude for either a higher target force or a shorter TTP.

There are several theories addressing the previously reported MFN results. Thus, brief descriptions of four of the most relevant theories regarding the MFN are given in the following chapter to provide a better understanding of the ERP component chosen to investigate the GMA.

2.4 Most relevant theories on the medial-frontal negativity

One of the first theories which tried to explain the MFN was the Mismatch Theory (Bernstein et al., 1995; Falkenstein et al., 1991). In this theory the MFN amplitude is a result of a comparator system that evaluates differences between the intended response and the actual outcome (Gehring et al., 2012).

Another influential theory was the reinforcement learning theory of the MFN (Holroyd & Coles, 2002). This theory postulated that the MFN is the result of an evaluation process as well, but, contrary to the Mismatch Theory, the evaluation process is here carried out on the subcortical level of the basal ganglia. According to the theory, the basal ganglia are producing an error signal (based on the so-called prediction error), which is transferred from the basal ganglia through the mesencephalic dopamine system to the anterior cingulate cortex (ACC). Eventually, the MFN amplitude is influenced by this signal of behavioural adjustment (Gehring et al., 2012; Holroyd & Coles, 2002).

The response conflict theory, as a further important theory, is based on the assumption that the ACC is sensitive to response conflict (Botvinick et al., 2001; Carter et al., 1998; Yeung et al., 2004). This theory postulates, contrary to the theories described previously, that the process which elicits the MFN is not only about error detection but rather about the size of the response conflict (Gehring et al., 2012).

Lastly, the Force Unit Monitoring Model (Armbrecht et al., 2013) takes the force production parameters (PF and TTP) into account. Accordingly, in this model the shape of the MFN is correlated with the physical effort made by a brief button press. Depending on how much force production motor units and therefore muscle fibres are activated, the action monitoring system in the ACC must be more or less active. This seems to be reflected in the MFN (Armbrecht et al., 2013).

2.5 Classical methods for ERP component quantification

There are three scoring methods for the statistical analysis of ERP components which are usually used. All three component quantifications, namely the peak amplitude, the mean amplitude, and the peak latency (Clayson et al., 2013), have strengths and weaknesses (see chapter 2.6). Through both the peak amplitude and the mean amplitude measurement, ERP researchers can examine if there is a significant difference in the "brain response" for the conditions of interest (e.g. correct responses vs. erroneous responses). The peak latency identifies when the investigated component appeared in time, and if there is a significant temporal lag between different conditions (Clayson et al., 2013; Luck, 2014).

The oldest method to quantify ERP amplitudes is the peak amplitude measurement (Luck, 2014). It is described as the most negative (or positive) point in a waveform within a specific time window. The peak amplitude is commonly determined within two steps. First, the researcher must specify the search window in which the location of the peak is assumed. Secondly, the peak within this search window must be defined. Hoormann et al. (1998) outlined that the search window should be wide enough to include all peaks of the chosen component, whereas it should exclude all neighboured peaks of the same polarity at the same time. For the determination of the peak amplitude, the maximum positive or negative voltage in the chosen search window is usually used. Luck (2014) describes this as the *simple peak amplitude.* He further distinguishes another peak amplitude measurement, the *local peak amplitude.* This amplitude measurement is defined as "the largest point in the measurement window that is surrounded on both sides by lower voltages" (Luck, 2014).

The mean amplitude is computed through averaging the voltage over a specific time window. The size for the time window can be determined by looking at the grand average waveform for the condition of interest (i.e. average of single-subject averages) or based on previous research (Clayson et al., 2013; Luck, 2014). The mean amplitude is not to be confused with the area amplitude. These two quantification methods are almost equivalent, but the area amplitude is not divided by the duration of the chosen time window as the mean amplitude.

Thus, using the mean amplitude, researchers get microvolt (µV) as an easy interpretable unit instead of units that multiply amplitude and time (µV·ms; Clayson et

al., 2013; Kappenman & Luck, 2012). Keil et al. (2014) suggested using the terminology positive area or negative area (for positive or negative polarity), integrated area (subtracting the positive area from the negative area or vice versa), and geometric area (adding the positive area to the negative area, Figure 2).

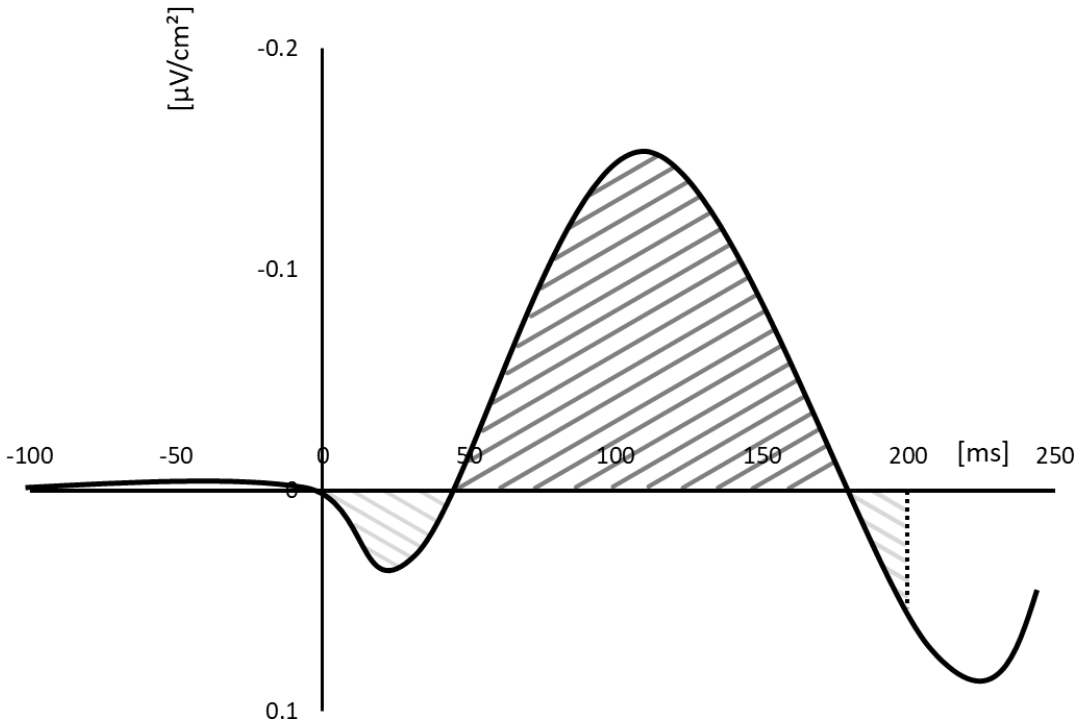

Figure 2. Illustration for the suggested terminology from Keil et al. (2014). In this example, the area is measured from 0 ms to 200 ms. The negative area corresponds to the dark grey dashed area. The integrated area is the light grey dashed area subtracted from the dark grey area. The geometric area is the light grey area added to the dark grey area.

The peak latency is the time point of the measured *simple peak amplitude* or *local peak amplitude* and is one possibility of representing the timing of a component (Clayson et al., 2013; Luck, 2014). Another possibility is to assess the timing of a component through a fractional area latency. For this, the measured area has to be divided in a specific set of fractions, most frequently the time point “at which the area under the curve is divided into equal halves” (Clayson et al., 2013).

The following section is focused on the peak amplitude, mean amplitude, and peak latency, because these are by far the most frequently used methods to quantify ERP components in ERP research (Clayson et al., 2013). Each of the introduced methods has its disadvantages, however, and some of the most important are briefly discussed.

2.6 Weaknesses of the classical methods

One of the most important points of criticism regarding the peak amplitude is that it is only a one-point measure of the ERP component. Therefore, the peak amplitude cannot be an appropriate representation of neural activity reflecting a sustained cognitive process (Luck, 2014; Woodman, 2010). Luck (2014) even goes so far as to say that “there is nothing special about the point at which the voltage reaches a local maximum” (p. 286). Moreover, the peak is at a different time-point for each participant in every single trial. This variability – the so-called latency jitter – results in smaller peak amplitudes for averaged waveforms, which is especially a problem if there is more latency jitter in one condition compared to the other conditions. Further, the peak amplitude is extremely sensitive to noise in the recorded EEG data (Luck, 2012, 2014; Woodman, 2010). Noisier data results mostly in larger peak amplitudes, because the noise superimposes the true EEG signal (McGillem et al., 1985). Therefore, averaged waveforms with a lower trial number are noisier than averaged waveforms with a higher trial number. Hence, the peak amplitude is a biased measurement which should not be obtained if there are conditions with larger differences regarding noise. One possibility to compensate for this bias could be balancing the trial numbers for all relevant conditions. However, it proves to be almost impossible to get equal trial numbers for all relevant experimental conditions (e.g. oddball experiments; Luck, 2012; 2014). These disadvantages make the peak amplitude an invalid method to quantify ERP components, particularly in conditions with unbalanced trial numbers or a greater latency variability in one condition than another. Clayson et al. (2013) thus came to the conclusion that this quantification method “should rarely be used” (p. 185).

One main reason why it is still used, however, seems to be its economic use. As it is an easy and fast measurement, historically it proved to be the method of choice, especially when researchers only had slow or even no personal computers and needed “nothing but an x-y plotter, a ruler, and enough time” (Donchin & Heffley, 1978). The point of criticism regarding the noise for the peak amplitude also applies to the peak latency. As described, it is the time-point of the measured peak amplitude. Thus, increased noise will also bias the peak latency measurement, because the true ERP peak is distorted (Clayson et al., 2013; Luck, 2014). The mean amplitude, however, is less sensitive to noise than the peak amplitude (Clayson et al., 2013) and more than just a point in time which defines the maximum voltage. Thus, the mean amplitude can capture more parts of an ERP component.

Nevertheless, it can be influenced by the selected time window, especially when the latency varies across conditions. In such cases, the method might not capture the “true” amplitude (Clayson et al., 2013; Kappenman & Luck, 2012; Luck, 2014). Consequently, the mean amplitude is the recommended method to quantify ERP components despite its restrictions (Luck, 2014). None of the scoring methods can capture the entire component in its size and shape. Almost all extractable information about the component’s shape, such as its rise and decline, cannot be analysed. These individual differences could reflect neuroanatomical variations or reflect differences in processing related to specific personality variables, behaviour, or other variables worth investigating (Kappenman & Luck, 2012; Luck, 2014). So far, variations in the sizes and shapes of ERP components have rarely been analysed systematically. There are some notable exceptions, however, for example Kiesel et al. (2008), who evaluated promising techniques to determine onset latencies (e.g. fractional area technique, jackknife- based approach). The authors stressed that they could only give rough recommendations, however, and that researchers always have to take the visual appearance of the ERP waveform into account. As such, this promising technique to estimate onset latencies has its limitations and does not provide information regarding the shape of the waveform.

Other approaches include modelling ERP components as a joint model of behavioural and neuronal data, functional data analysis to identify meaningful variations in brain activity through fitting basis splines to EEG data (Thivierge, 2007), and dynamic causal models to investigate underlying neuronal dynamics (David et al., 2006; Kiebel et al., 2006). There are also statistical methods to uncover hidden factors or sources of ERP data such as independent component analyses (ICA; Makeig et al., 1996) or correcting latency variability (i.e. residue iteration decomposition, RIDE; Ouyang et al., 2011). However, none of these approaches aim to model the entire shape of an ERP component.Mathematical modelling - that is, fitting mathematical models that describe the ERP components - might offer a solution to this problem. For example, Verleger and Wascher (1995) fitted an ex-Gauss function to individual ERP components (P3s) to investigate latency changes. By using the mean, the standard deviation, and the right skewness of the individually fitted ex-Gauss functions to their participant data, they were able to describe the characteristics of the P3 component.

3 The Gamma Model Analysis

In the following chapter, the GMA is introduced as an additional procedure for measuring ERP. In order to do so, firstly the gamma PDF will be explained. Secondly, the used grid restrained nelder-mead algorithm (Bűrmen et al., 2006) will be briefly described, followed by a more detailed explanation of how the GMA works, using both the Gamma PDF and the grid restrained nelder-mead algorithm.

3.1 The gamma probability density function

Around 1811, Adrien-Marie Legendre established the name “gamma function” and the associated symbol Γ. It is based on the generalisation of the factorial function to nonintegral values from Leonhard Euler (Bonnar, 2014).

$$\Gamma(x) = \int_0^\infty t^{x-1}\, e^{-t} dt \qquad x>0. \tag{1}$$

The gamma distribution with its PDF (see Equation 1) is used to model several processes statistically, for example the distribution of waiting times for customers or amounts of daily rainfall in a region (Krishnamoorthy, 2016). The following part is taken from Kummer et al. (2020).

The gamma PDF provides an excellent candidate to model ERP components, and it has already been applied to create simulated waveforms of single-trial lateralised readiness potentials (Stahl, Gibbons & Miller, 2010). A standard gamma PDF is given by:

$$F(t) = \begin{cases} 0, & t < 0 \\ a\left(\frac{r^k}{\Gamma(k)} t^{k-1} exp^{-rt}\right), & t \geq 0. \end{cases} \quad (2)$$

with the *rate parameter* ($r > 0$), and *shape parameter*[1] ($k > 0$) as functions of *time* ($t > 0$). Additionally, the function is scaled by a *scaling factor* ($a > 0$).

The gamma function is sufficiently flexible to fit waveforms with a rapid rise and a slow decline – a shape that is typical of most ERP components (Stahl, Gibbons & Miller, 2010). As subsequently demonstrated by fitting a gamma function to averaged ERP components, one obtains parameters that can be used as estimates of the ERP components' shape. The GMA provides three types of parameters, *basic parameters* (shape parameter, rate parameter, scaling), *time-dependent parameters* (first inflection point, mode, second inflection point), and *shape-dependent parameters* (skewness, excess). The three basic parameters are essential for the model fitting process; that is, values of these parameters are estimated so that the gamma function models the observed waveforms as closely as possible (details will be given below). The other parameter types are derived from the basic parameters (the shape and rate parameter; see Equations 2 to 6). Hence, the essential information of two basic parameters is contained in the time- and shape- dependent parameters. The scaling parameter is a special case which is only required for the fitting process by adjusting the overall size of the gamma function to the ERP components' shape.

The time-dependent parameters describe the temporal course of the waveform through the first inflection point (IP), the mode, and the second IP, whereas the skewness and the excess reflect shape characteristics of a waveform more specifically.

[1]The term 'shape' is used to refer to the shape of the function conceptually, but the term 'shape parameter' for the parameter *k* of a specific gamma function.

The *mode* reflects the point in time of the maximum peak of a gamma waveform and is defined as

$$Mode = k - 1/r \,,$$

for all $k \geq 1$. (3)

The *skewness* (*Q*), a measure of the asymmetry of the distribution, is defined as

$$Q = 2/\sqrt{k} \,.$$

(4)

The *excess* (*K*), a measure of the tailedness of the distribution, is defined as

$$K = 6/k \,.$$

(5)

The *first* and *second IPs*, the points of the distribution where the curvature changes its sign, when the convex (upward) aspect of the curve becomes concave (downward), or vice versa, are defined as

$$IP = (k - 1 \pm \sqrt{k-1})/r$$

for $k > 2$. (6)

Note that the time and shape dependent parameters cannot be interpreted independently as they are derived from the same basic parameters (k, r). Note that Equations 3 to 6 refer to the data point (s) and need a transformation to time (usually ms) in case the sampling rate is different from 1000 Hz.

Figure 3 illustrates how variations of the time- and shape parameters of the gamma distribution affect the shape of the distribution. As can be seen, a smaller shape parameter *k* results in waveforms with earlier mode and earlier IPs and a higher skewness and excess, which means more right-tailed waveforms with thicker tails (Figure 3 left panel). A smaller rate parameter *r* in turn results in waveforms with a later mode and later IPs and has no effect on the skewness or excess (Figure 3 right panel).

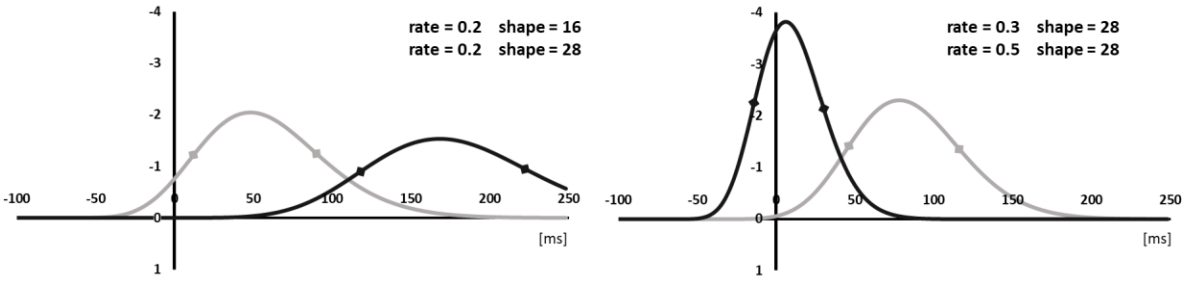

Figure 3. Gamma waveforms with varying shape parameter scores (left panel), and rate parameter scores (right panel), both with a fixed scaling and marked inflection points.

3.2 The grid restrained nelder-mead algorithm

The used grid restrained nelder-mead algorithm is derived from the original nelder-mead (NM) algorithm, which was published by Nelder and Mead (1965). The original NM algorithm is a direct search function (optimisation method), which tries to find a minimum of a scalar-valued nonlinear function with *n* real variables. To put it simply, the algorithm is looking for a set of variables where the value of a given function is the lowest through multiple iterations.

In each iteration, the algorithm operates by generating a geometric simplex (polytope) with *n* + 1 vertices (Figure 4, indicated by the grey dots). Each vertex consists of a set of *n* different real variables. Accordingly, the NM algorithm would generate a 3-simplex with four vertices (triangular pyramid) for the Gamma PDF described above, because it includes three different parameters (rate, shape, scaling).

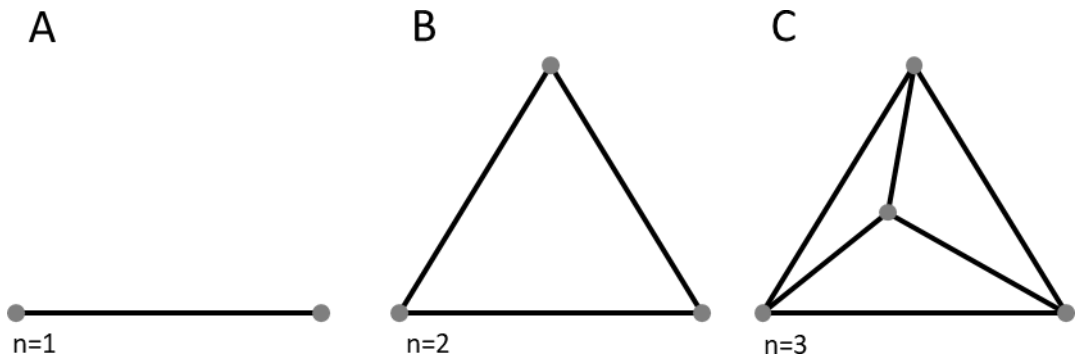

Figure 4. Three different geometric simplices with different number of vertices. (A) 1-simplex with 2 vertices - line segment (B) 2-simplex with 3 vertices - triangle (C) 3-simplex with 4 vertices - triangular pyramid. The grey dots mark the vertices.

The NM algorithm processes the used function at each of the vertices for the given variables. After that, the results of the function are sorted from the worst (fewest desirable values) to the best (most desirable values). Then, the NM algorithm tries to replace the vertex with the worst result with new variables through a transformation based on five different patterns, namely reflection, expansion, outside contraction, inside contraction, and shrinkage (Figure 5). Reflection means that the worst vertex is mirrored through the centroid of the remaining vertices, expansion would expand the reflected vertex, and an outside contraction reduces it. If these three patterns do not show a better result than an inside contraction, reducing the initial worst vertex, would be executed.

A shrinkage, reducing the initial simplex towards the best vertex, would be made, if previous transformations failed. The newly created simplex after the transformation process is used as a starting point for the next evaluation of the vertices.

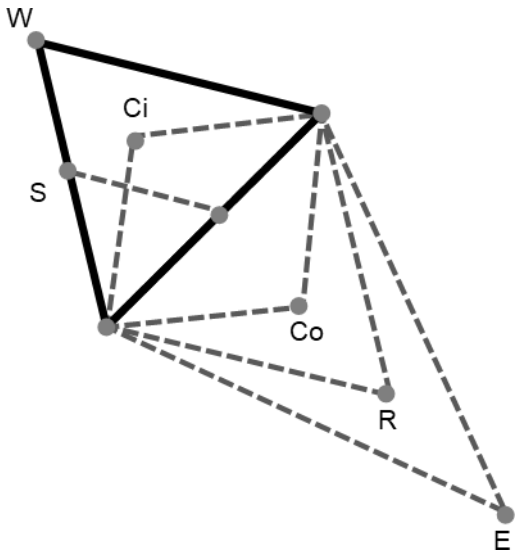

Figure 5. Nelder-Mead simplex steps. A triangle with the vertex for the worst result W, which is either transformed through reflection (R), expansion (E), outside contraction (Co), inside contraction (Ci), or shrinkage (S). Adapted from *Nelder-Mead User's Manual* by M. Baudin, 2010, *Consortium Scilab – Digiteo*, p. 47.

According to Wright (1996), two criteria are typically used to terminate the NM algorithm: "either the function values at the vertices are close, or the simplex has become very small" (p. 196; for details see Lagarias et al., 1998). This means that either the algorithm cannot find any more relevant difference between the different evaluations of the given function or the overall evaluation for all simplices can be described as small enough. The NM algorithm only converges slowly and cannot always guarantee a global convergence (Lewis et al., 2000). Therefore, Bűrmen et al. (2006) published a convergent variant of the NM algorithm using the principles of grid restrainment. They restricted the examined parameters of the vertices to a specific grid, which can be improved by fulfilling specific conditions (for details see, Bűrmen et al., 2006). Thus, the grid restrained nelder-mead algorithm is used for the GMA, because it is more reliable than the original NM algorithm. The algorithm is customised to use the three basic gamma PDF parameters (shape parameter, rate parameter, scaling) as input for the GMA.

3.3 The gamma model analysis

Initially a Gamma PDF is fitted to an input waveform (see Equation 2) with the rate parameter *r*, shape parameter *k* and scaling factor *a*. Is the component of interest represented in the input waveform negative, the Gamma PDF must be inverted.

As this is the first time to use GMA, there is no empirical evidence of reasonable starting parameters for the search algorithm. Consequently, the GMA starts with a broad range of starting parameters in a first pre-search to narrow down the search space. Up to 5,000 iterations were performed to derive appropriate starting parameters for the main search. Without the pre-search, the still unlimited parameter space would have been likely to have impacted negatively on our main search and to have resulted in a deadlock. To this end, uniformly distributed random values for the three parameters of the function for every iteration (rate parameter: 0 to 500, shape parameter: 0 to 500, scaling: 0 to 500) are determined. Based on these randomly drawn values, a Gamma PDF with the same length of the input waveform in data points is calculated and compared with the input waveform by calculating the root mean square error (RMSE; Barnston, 1992). A new Gamma PDF with a specific RMSE for every iteration is obtained for every iteration. If an RMSE is smaller than the previous iteration, the GMA keeps the parameters of this specific function and discard the previous parameters. The pre-search procedure is repeated until no smaller RMSE is found.

With the starting parameters from the pre-search, the finer main search determines the best-fitting Gamma PDF to the ERP waveform by using the adjusted grid-restrained nelder-mead algorithm (Bűrmen et al., 2006). These parameters were altered by the algorithm to find the smallest RMSE between the gamma waveform and the ERP waveform as described above. The parameters (basic, time-dependent, shape-dependent) of the Gamma PDF with the smallest RMSE are obtained. The obtained parameters are transformed from data points to ms.

A sanity check is performed by estimating whether the mode parameter fell within a reasonable time window (the time window is customizable). Obtaining a mode parameter outside this time window would indicate that the GMA did not fit the input waveform correctly, and the fit would be marked as an unsuccessful mode match. Data with unsuccessful mode matches can be excluded from the analyses.

4 Study 1: Simulation Study

Before fitting empirical data, a simulation study to evaluate the approach is conducted. The objective of the simulation study was to examine if it was possible to fit a Gamma PDF to simulated ERPs with varying noise levels. This made it possible to test whether the gamma model fitted the true ERP waveform and to ensure that it did not just fit the noise in the signal. Further it was examined whether a simulated effect, leading to differences in waveforms between two artificial conditions, would be reflected in the gamma model (GaM) parameters, providing support for the sensitivity of the approach to detect meaningful differences (which would be caused by differences in cognitive processes in real data).

4.1 Method

4.1.1 ERP Simulation

To systematically evaluate the susceptibility of GMA to EEG noise, an ERP waveform with a negative sign was simulated to provide a 'true' waveform without noise. This artificial ERP component consisted of a gamma waveform covering -100 ms before to 250 ms after the onset of the simulated event (Figure 6). To simulate an effect between two conditions, a *first condition* (A) is simulated, where *n* individual gamma waveforms with varying basic parameters (shape parameter: 20 ± 5; rate parameter: 0.2 ± 0.05; scaling parameter: 200 ± 50; sample size *n* = 100) are used; these variations reflected realistic varying averaged single-subject ERP components. The *second condition* (B) was simulated identically, but with larger shape parameters on average (25 ± 5) for every simulated participant. This resulted in simulated effects for every time-dependent and shape-dependent parameter. Overall, a variability of the GaM parameters of interest using this approach was obtained, and a known (i.e. 'true') effect between two conditions, which should be identified by the subsequent GMA.

The simulated EEG noise was created in a similar way to previous ERP simulation studies (Clayson et al., 2013; Gratton et al., 1989; Yeung et al., 2007). Fifty randomized sinusoids to simulate background EEG noise were summed. The sinusoids ranged in frequency from 0.1 to 125 Hz and had a fixed sampling rate of 1000 Hz. The maximum amplitude of any single sinusoid was randomly varied within a range of maximum amplitude parameters (0.1 µV to 1 µV). In three runs, the range increased from 1 µV to 3 µV and further up to 6 µV to evaluate the effects of increased noise on the GMA.

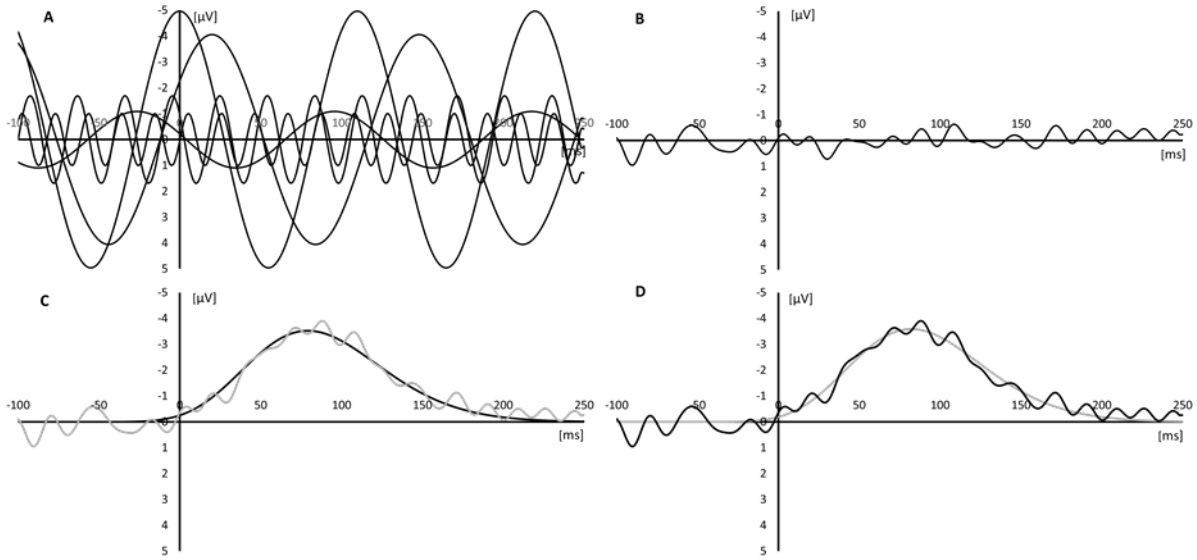

Figure 6. Main steps of the simulation procedure: (A) illustration of five phase-randomized noise sinusoids of various amplitudes and frequencies (note: 50 were used in the simulation) with a maximal amplitude range from 0.1 µV to 6 µV; (B) average of noise sinusoids; (C) the solid black line shows a simulated 'true' ERP waveform, the grey line shows the noisy 'true' ERP waveform (sum of true ERP and averaged noise waveform); (D) the solid black line shows simulated 'true' ERP waveform with noise, the grey line shows the resulting gamma waveform after the GMA.

4.2 Simulation procedure

The averaged ERP waveform of one simulated 'individual', with noise and without noise, was constructed as described above. This procedure was separately performed for 100 averaged ERP waveforms. In the next step, the range of maximum noise amplitude was increased. The range of maximum noise amplitude started with a lower boundary of 0.1 µV and an upper limit of 1 µV. The lower boundary was kept, and the upper limit was increased from 1 µV to 3 µV and 6 µV.

The amplitude of noise could vary randomly within the defined range. Consequently, three noise levels with 100 simulated individuals in two conditions were obtained, which resulted in 600 individual waveforms.

4.2.1 Gamma model analysis

The simulated averaged ERP waveforms from each simulated ‘individual’ for the GMA were used. The reasonable time window for the sanity check was defined from the simulated response onset to the end of the simulated event (0 ms to 250 ms). Everything else worked as described in Section 3.3.

4.2.2 Data analysis

Several dependent *t*-tests with the two simulated conditions (without noise) as the independent variable and the simulated GaM parameters as dependent variables to determine the ‘true’ effect were used. An *estimation bias* for all GaM parameters, which was defined as the difference between the ‘true’ GaM parameters of our simulated waveforms and the estimated GaM parameters from our GMA approach, was calculated. This was performed for all simulated waveforms, separately for the simulated conditions. Two-way analyses of variances (ANOVAs) were performed with the within-subject factors noise level (1 vs 3 vs 6 [µV]) and simulated condition (A vs B) for GaM parameters. Within-subject effects were analysed using Tukey’s HSD post hoc tests.

4.3 Results

4.3.1 Size of the 'true' effect

Separate *t*-tests for each simulated GaM parameter with the simulated condition as the independent variable were performed. The *t*-tests revealed significant effects for all GaM parameters (all *p*s < .01; Table 1).

Table 1. *t*-value and *p*-value for the time-dependent and the shape-dependent simulated gamma parameters (first IP, mode, second IP, skewness, excess; N=100).

	t	*p*	*r*
Time-dependent parameters			
First Inflection Point	-8.56	<.01	.65
Mode	-8.00	<.01	.63
Second Inflection Point	6.77	<.01	.56
Shape-dependent Parameters			
Skewness	12.08	<.01	.77
Excess	11.95	<.01	.77

GMA successfully identified in the second condition the later first inflection point, the later mode and the later second inflection point compared to the first condition. Curves in the first condition were also more right-tailed and had thicker tails (for all means and standard deviations see Table A1, appendix).

4.3.2 Estimation bias and simulated conditions

The estimation biases between the 'true' GaM parameters and the estimated GaM parameters for all three noise levels (Figure 7) show that the mean estimation biases were around zero, and more importantly, the means did not vary systematically with increasing noise level for any of the GaM parameters.

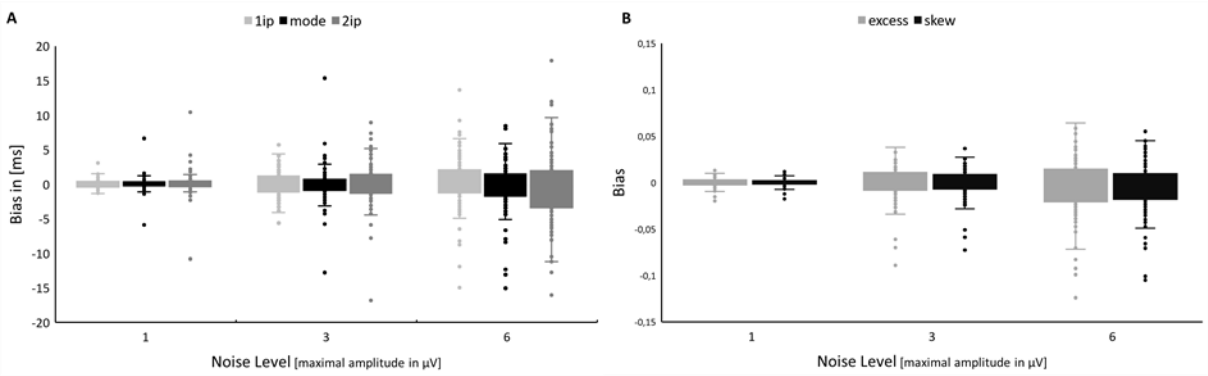

Figure 7. (A) Estimation biases (i.e. 'true' parameter minus estimated parameter) in ms for the time-dependent gamma model parameters as box plots displayed separately for the three noise levels; the light grey boxes show the bias for the first IP, the black boxes show the bias for the mode and the dark grey boxes show the bias for the second IP; (B) calculated biases for the shape-dependent gamma model parameters as box plots displayed separately for the three noise levels; the light grey boxes show the bias for the excess and the black boxes show the bias for the skewness (Kummer et al., 2020).

As expected, the standard deviations of the estimation biases increase linearly with increasing noise level for each GaM parameter (for all means and standard deviations see Table 2).

Table 2. Mean, standard deviation (± *SD*) for the bias of the time-dependent and the shape-dependent gamma model parameters (first IP, mode, second IP, skewness, excess) for every noise level (N=600).

Noise Level	1	3	6
Estimation Bias			
First Inflection Point	-0.02 ± 0.64	-0.13 ± 2.29	1.05 ± 8.80
Mode	-0.08 ± 0.80	-0.19 ± 3.57	0.49 ± 12.71
Second Inflection Point	-0.14 ± 1.36	-0.26 ± 5.95	-0.19 ± 18.24
Skewness	<0.01 ± <0.01	<0.01 ± 0.013	<0.01 ± 0.035
Excess	<0.01 ± <0.01	<0.01 ± 0.016	<0.01 ± 0.033

The ANOVAs for each estimated GaM parameter with the within-subject factors' simulated condition and noise level revealed no significant main effects for the noise level (all *p*s > .05). The analyses revealed significant effects for the simulated condition (with noise) for all GaM parameters (all *p*s < .05). The GMA identified again in the second condition a later first IP, a later mode and a later second IP point than in the first condition. Furthermore, curves in the first condition were more right-tailed and had thicker tails (for all means and standard deviations see Table A1, appendix). The interactions between the simulated condition and noise level revealed no significant effects (all *p*s > .05; for effect sizes and details, see Table A2, appendix).

4.4 Discussion

The main objectives of the simulation study were to examine the reliability and validity of the GMA. To this end, Study 1 tested whether the GMA was able to fit Gamma PDFs to simulated noisy ERPs and whether a simulated effect could be recovered despite the presence of noise. First, Figure 7 shows that the standard deviations of the estimation biases for the parameters increased linearly with the increasing noise level, indicating that the measurement was less reliable with more noise in the signal, which is to be expected. More importantly, however, the validity of the GMA was demonstrated because the mean estimation biases varied around zero for all three noise levels. This means there was no systematic over- or underestimation due to the presence of noise, thereby providing strong support for the GMA's ability to recover the true shape of the curve even when noise levels increased.

The GMA was also able to reliably identify the known (i.e. induced) effect between conditions, and the noise level showed no main effect on, or interaction with, the simulated conditions in any of the GaM parameters. Again, the presence of noise did not affect the estimation of the GaM parameters systematically, which may mitigate possible concerns that the GMA may just fit noise rather than ERP components. Having demonstrated the reliability/validity of the GMA in fitting simulated ERP waveforms, the goal of Study 2 was to evaluate whether the GMA was also able to fit empirical waveforms and to explore whether the GMA is related to behavioural variations.

5 Study 2: Flanker Task

Study 2, as following, is taken from Kummer et al. (2020). For the second evaluation of the GMA, data from a large-scale study with a flanker task, which is a well-established paradigm for investigating error processing and variations in MFN (Bode & Stahl, 2014) was reanalysed. The objectives of this study were to examine whether the GMA was able to fit a Gamma PDF to the ERPs and to explore response-type effects (error vs correct) on the GaM parameters.

5.1 Material and methods

5.1.1 Participants

A total of 121 participants originally took part in the study (109 of those were included in Bode and Stahl (2014), which required a specific number of trials for the applied analyses; for a detailed description see their Method). To be included in the analyses for the present paper, a participant's data set had to contain at least six usable trials (after EEG artefact removal) for each condition. Two data sets were removed because they were marked as unsuccessful mode-peak matches by the GMA (for details see below), and a further six data sets had to be excluded as extreme outliers corresponding according to Tukey fences (1977). The final sample contained 113 (65 female) participants; their age ranged from 19 to 49 (M = 25.80; SD = 6.55). The study was approved by the ethics committee of the German Psychological Society (DGPs), and the study was conducted according to the Declaration of Helsinki.

5.1.2 Apparatus

The custom-made response keys, which were used to assess the response time and the response force, were composed of a plastic cuboid (110 mm x 619 mm x 62 mm) attached to a spring steel plate held by an adjustable metal clamp at one end. Individually adjusted boards were located on the left and right sides of the computer screen, on which the participants rested their forearms and palms while both fingertips of their index fingers rested on the open end of the cuboid. The location and posture of the participants were kept constant by using an adjustable chin rest (at a 56 cm distance from the monitor).

The response force of the index finger was measured by strain gauges at the fixed end of the cuboids. The analogue signal was digitized at a sampling rate of 500 Hertz.

5.1.3 Procedure

Participants performed a digit flanker task (Stahl, 2010). A typical trial sequence of the task is depicted in Figure 8 (left side). Specifically, in each trial, a row of three white digits was presented in the centre of a black screen for 67 ms, and the participant had to respond to the parity of the central digit (1 to 8). Two identical digits (1 to 8), which were different from the central digit, were shown as flankers, one on each side. These were either congruent or incongruent in relation to the parity of the central digit (e.g. ‘262’ or ‘474’). The assignment of response hand to parity decision was counterbalanced across participants. Depending on the response, one of the three feedback types was presented for 200 ms: ‘R’ (‘richtig’, German for ‘correct’) indicated a correct response; ‘H’ indicated a ‘hand error’ (incorrect response, hereafter simply referred to as ‘error’); and ‘Z’ (‘Zeit’, German for ‘time’) indicated slow responses. Slow responses (i.e. beyond the response time window: 90% of a participant’s average response time in a practice block) were excluded from the analyses. The feedback screen was followed by a 1500 ms black screen before the onset of the next trial. Overall, participants completed one practice block and 10 experimental blocks, each block comprising 40 trials (20 congruent and 20 incongruent in random order). For five blocks, participants were instructed to respond as fast as possible; for the other five, they were instructed to respond as accurately as possible. The order of speed and accuracy blocks was counterbalanced across participants. To maximize the number of trials per condition, the data from the speed and accuracy blocks for the current analysis was aggregated.

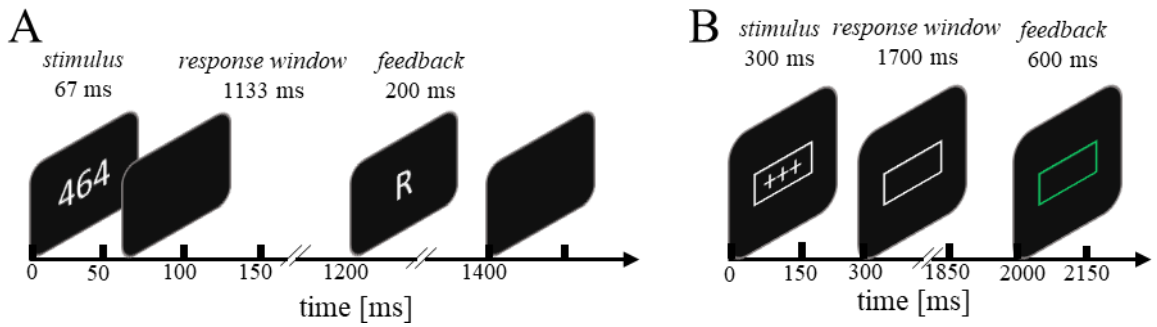

Figure 8. Time course of the paradigms of Study 2, (A) a digit flanker task and Study 3, (B) a force production task (for details see the method sections; Kummer et al., 2020).

5.1.4 Behavioural data

The median response time (RT) was defined as the median of the time interval between the onset of stimulus presentation and the first response force exceeding 50 cN. Two response force parameters were extracted, the PF and TTP. The PF was defined as the peak amplitude of the force curve after response onset in each trial. The TTP was defined as the time interval between response onset and the time point at which the PF was reached.

5.1.5 Electrophysiological data

EEG Recording. The EEG was recorded with 61 Ag/AgCl electrodes (Fp1, Fp2, AF7, AF3, AF4, AF8, F7, F5, F3, F1, Fz, F2, F4, F6, F8, FT7, FC5, FC3, FC1, FCz, FC2, FC4, FC6, FT8, T7, C5, C3, C3', C1, Cz, C2, C4, C4', C6, T8, TP7, CP5, CP3, CP1, CPz, CP2, CP4, CP6, TP8, P7, P5, P3, P1, Pz, P2, P4, P6, P8, PO7, PO3, POz, PO4, PO8, O1, Oz and O2). The active Ag/AgCl electrodes (actiCAP, Brain Products) were referenced against the left mastoid and the ground was placed at AFz. Vertical and horizontal electrooculograms (EOGs) were recorded from electrode positions infraorbital to the left eye, and 2 cm lateral from the outer canthi. The EEG was continuously recorded at a sampling rate of 500 Hz using a BrainAmp DC (Brain Products) amplifier. An online band-pass filter (DC – 70 Hz) was employed for all channels. The components were derived from the FCz electrode position at the local maximum of the component.

EEG pre-processing. The EEG was analysed offline with epochs ranging from -100 ms to 400 ms after response onset. A baseline period of 100 ms preceding the response onset was used. The effects of eye blinks were eliminated by using the ocular correction algorithm of Gratton et al. (1983). All data were screened for artefacts, and contaminated trials exceeding maximum/minimum amplitudes of ±150 μV were rejected. Current source density (CSD; Perrin et al., 1989) transformations were implemented to reduce overlap of simultaneous activity of contiguous electrodes (e.g. Gibbons et al., 2011; Vidal et al., 2000; Vidal et al., 2003). The order of the splines was 4, the maximal degree of the Legendre polynomial was 10 and the λ regularization value was 1.0e-005.

The GMA can be applied to ERP waveforms with and without a CSD transformation because ultimately the GMA fits waveforms without considering any kind of mathematical transformation, and both waveforms are well described by Gamma PDFs. In general, CSD transformation has the advantage that it produces reference site-independent and more sharply localized components than the classical scalp potentials. The CSD transformation also removes the volume-conducted activity from other regions (Luck, 2014; Tenke & Kayser, 2005). In the present study, a CSD transformed waveforms were used because these were also used in the original study of Bode and Stahl (2014).

The data were segmented into epochs from -100 ms to 250 ms around the response onset and averaged for erroneous responses and correct responses. All amplitude measurements were determined from each participant's averaged ERP waveforms separately for each response type.

The response-locked MFN peak amplitude was determined as the most negative peak in a time window ranging from 0 to 150 ms after response onset. The response-locked MFN area was determined as the integrated area, the unrectified mean amplitude, in a time window ranging from 0 to 150 ms (Keil et al., 2014). The MFN latency was measured as 50% fractional area latency at the time point that divides the area into halves (Luck, 2014).

5.1.6 Gamma model analysis and statistical analyses

The GMA was performed identically to Section 3.3. Outliers of the GMA were determined by Tukey fences with the normalized RMSE as an exclusion criterion to detect possible far outliers. Tukey fences for one-sided far outliers are defined as the sum of the median of the upper half of the data and the interquartile range multiplied by three (Tukey, 1977). Goodness-of-fit analyses were performed by comparing the estimated gamma waveforms with the observed ERP waveforms by RMSE and correlating the two waveforms across the entire time range for all conditions. A *t*-test for the individual correlation coefficients to examine the (in)dependence of the goodness-of-fit analyses from the experimental variation was also used. The main analyses considered pairwise correlations between the individual ERP parameters, the GaM parameters, and the behavioural data. The reported correlation coefficients are Pearson's correlations (before averaging the correlation coefficients, a Fisher's *z* transformation was applied). Several *t*-tests were performed regarding response type (error vs correct) for the classical ERP parameters and the GaM parameters. All statistical analyses were corrected for multiple comparisons using the Šidák correction (Šidák, 1967).

5.2 Results

5.2.1 Goodness-of-fit analysis

The averages of the best-fitting gamma waveforms and empirical ERP waveforms at the FCz electrode site are depicted in Figure 9. The imperfect fits of the GMA to the tail end are discussed below. The individual correlations for erroneous responses ranged from $r = .66$ to $r = .99$ (mean $r = .90 \pm .41$) and from $r = .49$ to $r = .99$ (mean $r = .92 \pm .49$) for correct responses. The *t*-test showed no significant difference between the correlation coefficients for correct and erroneous responses, $t(112) = 0.97$, $p = .34$. The RMSE for erroneous responses ranged from RMSE = 0.012 to RMSE = 0.276 (mean RMSE = 0.076 ± 0.056) and from RMSE = 0.007 to RMSE = 0.106 (mean RMSE = 0.039 ± 0.020) for correct responses. The *t*-test showed a significant difference between the RMSEs for correct and erroneous responses, $t(112) = 8.17$, $p < .05$.

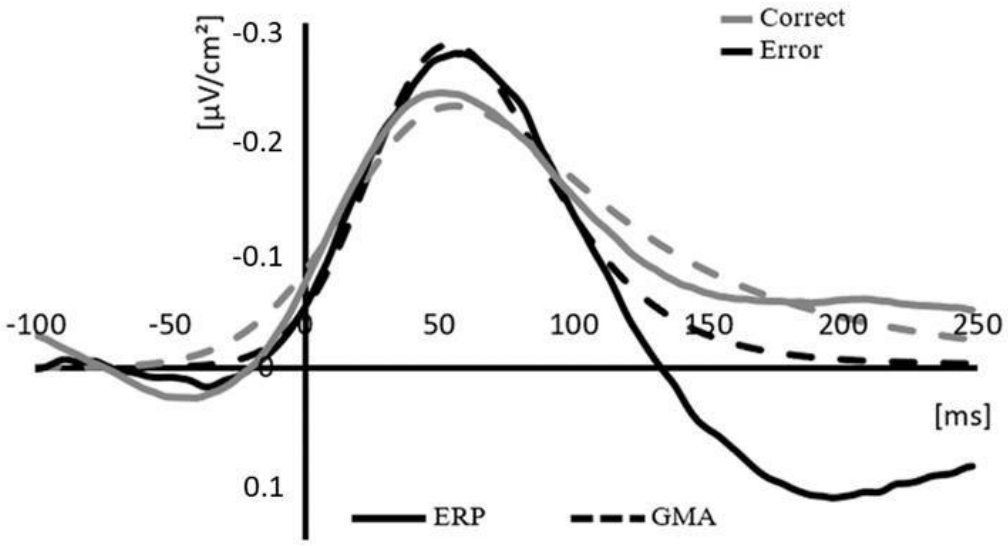

Figure 9. Grand average CSD-ERP waveform at electrode site FCz and averaged gamma waveforms for erroneous and correct responses extracted from the model fit. Negative values are plotted upwards and time point zero represents the response onset (Kummer et al., 2020).

5.2.2 Error rate

On average, the participants responded erroneously in 16.09 ± 5.83% of the trials.

5.2.3 Correlations with the behavioural data

The correlation analyses between the classical ERP parameters, the GaM parameters and the behavioural data were used to identify possible covariations between the behavioural parameters (median RT, PF, TTP) and all ERP parameters. The classical ERP parameters and the GaM parameters were also correlated to detect possible associations.

Classical analyses. There were no significant correlations between the classical ERP parameters and any of the behavioural data for correct responses (*r*s ranging from -.06 to .27, all *p*s > .0008; for details see Table A3, appendix). The PF showed a significant correlation with the latency ($r = .35$, $p < .0008$) for erroneous responses.

Gamma model analysis. There were no significant correlations between the behavioural variables and the GaM parameters for correct responses (*r*s ranging from -.18 to .18, all *p*s > .008; for details see Table A3, appendix). However, for erroneous responses, the PF showed several significant correlations (rate: $r = -.32$; mode: $r = .34$; second IP: $r = .34$; skewness: $r = .34$; excess: $r = .32$; all *p*s < .0008).

Overall, this pattern of correlations indicates that a higher PF was associated with a later mode and a later second IP in erroneous responses. The waveforms of erroneous responses were also more skewed to the right and more leptokurtic, with a higher PF or higher TTP.

5.2.4 Correlations between ERP parameters and GaM parameters

Table 3 shows all significant correlation coefficients between the classical ERP parameters and the GaM parameters (all *p*s ≤ .001; for all correlation coefficients see Table A4, appendix).

Table 3. Overview of all significant Pearson's correlation coefficients for the gamma model parameters with classical ERP parameters, separately for response type (error vs correct; N = 113). Corrected for multiple comparisons through Šidák correction (all *p*s ≤ .001)

	Error			*Correct*		
	Peak	Area	Latency	Peak	Area	Latency
Shape parameter						
Rate parameter		-.41	-.43	.37	-.51	-.47
Scaling	-.74	.85		-.81	.91	.44
Mode			.71			.59
2nd IP			.54			.60
Skewness			.35		.46	.47
Excess			.34		.41	.44

Note: For all correlation coefficients see Table A4, appendix.

Overall, the pattern of correlations for both correct and erroneous responses indicated that a more negative peak amplitude and a larger area were both associated with a higher scaling and lower rate parameter of the GMA. A longer latency was also associated with a lower rate parameter, with later time-dependent GaM parameters (mode and second IP), and with more right-skewed thicker-tailed waveforms.

A higher negative peak amplitude for correct responses was associated with a larger rate parameter. A larger area for correct responses was also associated with more right-skewed and thicker-tailed waveforms.

These results confirmed the close and reasonable relationship between classical ERP parameters and GaM parameters. The ERP parameters are usually used to investigate cognitive functions (e.g. investigating group-average differences between errors and correct response in the MFN time window), and so in the next step, this approach was applied to both the ERP parameters and the GaM parameters and compared their ability to identify behavioural experimental effects.

5.2.5 Event-related potentials

Classical analysis. Separate *t*-tests for each parameter of the classical ERP analysis were performed. The peak analysis showed a significant effect of response type, $t(112) = 4.08$, $p < .001$, $r = .36$. Specifically, erroneous responses had a larger negative peak (-0.31 ± 0.17 µV/cm²) than correct responses (-0.26 ± 0.14 µV/cm). The analyses of the area (correct: 0.16 ± 0.11 µV/cm²; error: 0.15 ± 0.10 µV/cm²; $p = .13$) and latency (correct: 56.96 ± 6.98 ms; error: 56.46 ± 6.25 ms; $p = .44$) showed no significant effects for response type.

Gamma model analysis. Several *t*-tests were conducted to examine the effect of the response type on each of the GaM parameters (Table 4). Figure 9 shows the gamma waveforms that were extracted from the model fit as a function of the response type. As can be seen in Table 4, erroneous responses had a larger shape parameter than correct responses. The erroneous responses also had a larger rate parameter. Finally, erroneous responses had smaller scaling parameters than correct responses.

Table 4. Mean, standard deviation (± SD), *t*-value, *p*-value and *r* for the gamma model parameters (shape parameter, rate parameter, scaling, first IP, second IP, mode, skewness, excess), separately for each response type (correct vs errors; N = 113). Corrected for multiple comparisons through Šidák correction.

Response Type	M	*t*	*p*	*r*
Basic Parameters				
Shape parameter				
Correct	19.09 ± 16.5	-5.81	< .006	.53
Error	28.87 ± 13.5			
Rate parameter				
Correct	0.23 ± 0.18	-6.02	< .006	.55
Error	0.36 ± 0.22			
Scaling				
Correct	1.28 ± 0.90	3.59	< .006	.33
Error	1.63 ± 1.18			
Time-Dependent Parameters				
First inflection point [ms]				
Correct	16.69 ± 21.0	-4.09	< .006	.38
Error	25.05 ± 13.0			
Mode [ms]				
Correct	67.78 ± 30.0	2.42	.02*	.21
Error	59.78 ± 24.1			
Second inflection point [ms]				
Correct	125.15 ± 57.8	4.22	< .006	.39
Error	97.10 ± 53.6			
Shape-Dependent Parameters				
Skewness				
Correct	0.56 ± 0.19	7.85	< .006	.71
Error	0.41 ± 0.12			
Excess				
Correct	0.52 ± 0.34	7.37	< .006	.67
Error	0.27 ± 0.22			

*non-significant: $p > .006$

For the time-dependent GaM parameters, the analyses showed significant effects for two parameters. Correct responses showed an earlier first IP and a later second IP compared to erroneous responses. There was no significant effect for the mode parameter. The analyses of the shape-dependent parameters showed significant effects for the skewness and excess parameters. As shown in Table 4, the skewness parameter was significantly larger for correct than for erroneous responses. The excess parameter was also significantly larger for correct than for erroneous responses.

Overall, the findings indicate that the ERP waveforms of correct responses had an earlier first IP, a later second IP and were more skewed to the right, with thicker tails compared to erroneous responses.

5.3 Discussion

Study 2 aimed to examine whether the GMA would generally be able to fit the shape of an empirical MFN and whether the GaM parameters would reasonably capture variations between the different response types (errors and correct response). The goodness-of-fit analyses showed high correlations between gamma waveforms and the ERP waveforms (on average, they explained 81% of the variance; R^2 ranged from 44% to 98%). The imperfect fits for some data sets and the significant differences between the RSMEs for correct and erroneous responses might be due to a possible sign change occurring at the tail of the component (see Figure 9), which results from an error-related positivity following the MFN. The Gamma PDF is not able to fit a sign change, which makes the fit not perfect at the end of the time window for single data sets. Despite this limitation, however, the GMA seemed to fit the observed waveforms very well.

Furthermore, the correlation analyses of the classical ERP parameters with the behavioural parameters showed only one significant relationship between the PF and the latency for erroneous responses. Interestingly, some time-dependent GaM parameters and the shape-dependent GaM parameters correlated significantly with behavioural parameters across participants; for example, errors with a higher PF had a later second IP and a later mode in the GaM parameters. Moreover, erroneous responses with a higher PF or a longer TTP showed stronger skewness to the right with thicker tails in the GaM parameters. Importantly, using the classical ERP parameters (peak amplitude, area, latency) only a relationship between PF and erroneous responses regarding the latency could be detected.

The correlation analyses between the ERP parameters and the GaM parameters revealed several interesting correlations. First, a later latency was associated with a later mode, a later second IP and a more right-skewed and thicker-tailed waveform. Second, a higher negative peak amplitude and a larger area were associated with a larger scaling parameter.

On the one hand, this shows the expected strong relationship between the modelled and the original component; on the other hand, as regards the behavioural measures, it also suggests that the GMA might provide a supplementary set of easily interpretable parameters in addition to the classical methods. For future research, all parameters (classical and GMA) could potentially be aggregated to interpret the ERP's shape.

Using GMA, our main goal was to identify the sensitivity of the GaM parameters to the two investigated conditions. Response-type effects for two basic parameters, the time-dependent parameters and the shape-dependent parameters were found. Most importantly, the time-dependent parameters showed an earlier first IP and a later second IP in correct trials compared to error trials. The analyses of the shape-dependent parameters also showed that correct responses were more skewed to the right with thicker tails. These observations could not be made by using classical ERP parameters. Thus, our approach could indeed provide additional insights into the rise and decline of a component's waveform in relation to the cognitive process of interest. Study 2 revealed some interesting correlations between behavioural parameters that were connected to force production (TTP, PF) and the GaM parameters. Thus, the observed associations with behavioural parameters such as TTP and PF were investigated in more detail by using the data of a force production task in the following section.

6 Study 3: Force Production Task

As some GaM parameters (e.g. skewness and excess) correlated with PF and TTP in Study 2, the data of a force production task in which participants produced a specific amount of force (low, high) with a short or long TTP was reanalysed (Armbrecht et al., 2013). The study investigated contradictory results for the MFN regarding the effects of force magnitude and errors in force production in previous research (Armbrecht et al., 2012; Bruijn et al., 2003). Armbrecht et al. (2013) developed a mathematical model based on the observation that the shape of the component varies with their experimental manipulations (e.g. a broader component in the longer TTP condition), which, however, could not be tested with the classical approaches.

The data of their study could thus serve as an appropriate test the GMA as the grand average waveforms showed clear variations in the shape of the components across conditions. It would be a strong demonstration of the benefits of the GMA if it was possible to identify and to statistically test such variations with GMA (e.g. testing mathematical models such as the model of Armbrecht et al., 2013). For the sake of brevity, the investigation focused only on the component's shape variations related to PF and TTP for errors. Additionally, because the scaling parameter has no informative value beyond the amplitude, and the interpretation of the basic parameters is less intuitive, only the time-dependent GaM parameters and the shape-dependent GaM parameters were analysed.

6.1 Material and methods

6.1.1 Participants

Twenty-four healthy students participated and either received course credits for their participation or were paid (€ 7.5/h). Three participants were excluded due to a low number of trials (< 6 after artefact removal), two participants were excluded because they were marked as unsuccessful mode-peak matches and one participant was excluded because the data was marked as a far outlier by Tukey fences (Tukey, 1977). The final sample contained 18 (11 female) participants (age ranged from 19 to 33; *M* = 23.28; *SD* = 3.88).

6.1.2 Procedure

The study contained two sessions: a practice session without EEG and the main experiment with EEG recording the next day (for details see Armbrecht et al., 2013). The participants were instructed to produce fast, isometric force pulses, which should peak within a specific target-force range (high or low; see below). The specific target-force ranges were determined individually. To this end, a participant's maximum voluntary force (MVF) was first determined (i.e. mean force of seven force key responses that were as strong as possible) for each hand separately. Based on the MVF, two target-force ranges were obtained. The target-force range for the low PF condition was 15–25 % of the MVF; the target-force range for the high PF was 34–56 % of the MVF.

In addition to the PF (high or low), the TTP (short vs long) was used as an independent variable while participants were asked to produce force pulses falling in the low or high force range and into a short (113 to 188 ms) or long TTP (300 to 500 ms) range. Crossing the two experimental factors (PF and TTP) resulted in four conditions: lowPF-shortTTP, lowPF-longTTP, highPF-shortTTP and highPF-longTTP. The conditions were presented block-wise.

The experiment included a total of 16 blocks (30 trials each) with four blocks (two for each hand) per condition. The participants had to produce one of the four force-TTP conditions (the order of the conditions was fully balanced across the participants). The first five trials of each block served as practice trials and were excluded from the analyses. A trial (Figure 8B) started with the presentation of a row of three white crosses (+++) on a black background (duration: 300 ms) as the starting signal in the centre of the white frame. Visual feedback was shown 2000 ms after stimulus onset. The feedback (red frame and green frame, 600 ms) indicated whether the force pulse was or was not within the required PF and TTP ranges. The instructions accentuated emphasized the response speed and accuracy equally (for more details, see Armbrecht et al., 2013).

6.1.3 Behavioural data, electrophysiological data

The behavioural data (median RT, TTP, PF) and the EEG data were recorded and pre-processed in the same way as in Study 2.

6.1.4 Gamma model analysis and statistical analysis

The GMA was performed identically to that the previous studies. Tukey fences outlier control and goodness-of-fit analyses were performed (see Study 2). Two-way analyses of variance (ANOVAs) with the within-subject factors Force Type (low vs high) and TTP Type (short vs long) for the within-subject correlation coefficients were performed to examine their independence from experimental variation. Correlation analyses were performed to investigate the individual variation in the ERP parameters and GaM parameters. The reported correlation coefficients are Pearson's correlations (correlations were Fisher's *z*-standardized before averaging). All analyses were corrected for multiple comparisons (Šidák, 1967).

Two-way ANOVAs were performed with the within-subject factors Force Type (low vs high) and TTP Type (short vs long) for the classical ERP parameters and GaM parameters.

6.2 Results

6.2.1 Goodness-of-fit analysis

Table 5 shows the mean, standard deviation, and range for all correlations and RMSEs of the goodness-of-fit analyses of the ERP waveforms and gamma waveforms (Figure 10).

Table 5. Mean, standard deviation (± *SD*) and range for Pearson's correlation coefficients and root mean square errors for the goodness-of-fit analyses comparing the estimated gamma waveforms with the observed ERP waveforms for all conditions of Study 4 (lowPF-shortTTP, lowPF-longTTP, highPF-shortTTP, highPF-longTTP; N = 18)

	Pearson's correlation		*Root mean square errors*	
	mean	range	mean	range
lowPF-shortTTP	.91 ± .12	.55 to .99	0.058 ± 0.068	0.020 to 0.113
lowPF-longTTP	.86 ± .11	.63 to .98	0.045 ± 0.055	0.020 to 0.095
highPF-shortTTP	.94 ± .12	.63 to .99	0.068 ± 0.077	0.014 to 0.144
highPF-longTTP	.89 ± .11	.62 to .98	0.045 ± 0.048	0.019 to 0.098

The ANOVA for the individual correlation coefficients showed no significant effects for Force Type, $F(1, 17) = 3.71$, $p = .07$, TTP Type, $F(1, 17) = 4.24$, $p = .06$ or their interaction, $F(1, 17) < 0.01$, $p = .99$. There were no significant RMSE effects for Force Type, $F(1,17) = 0.11$, $p = .75$ and the Force Type-TTP Type interaction, $F(1,17) = 0.19$, $p = .67$. For the TTP Type a significant effect was found, $F(1,17) = 13.54$, $p < .01$, meaning that larger RMSEs were found for responses with a short TTP than for responses with a long TTP.

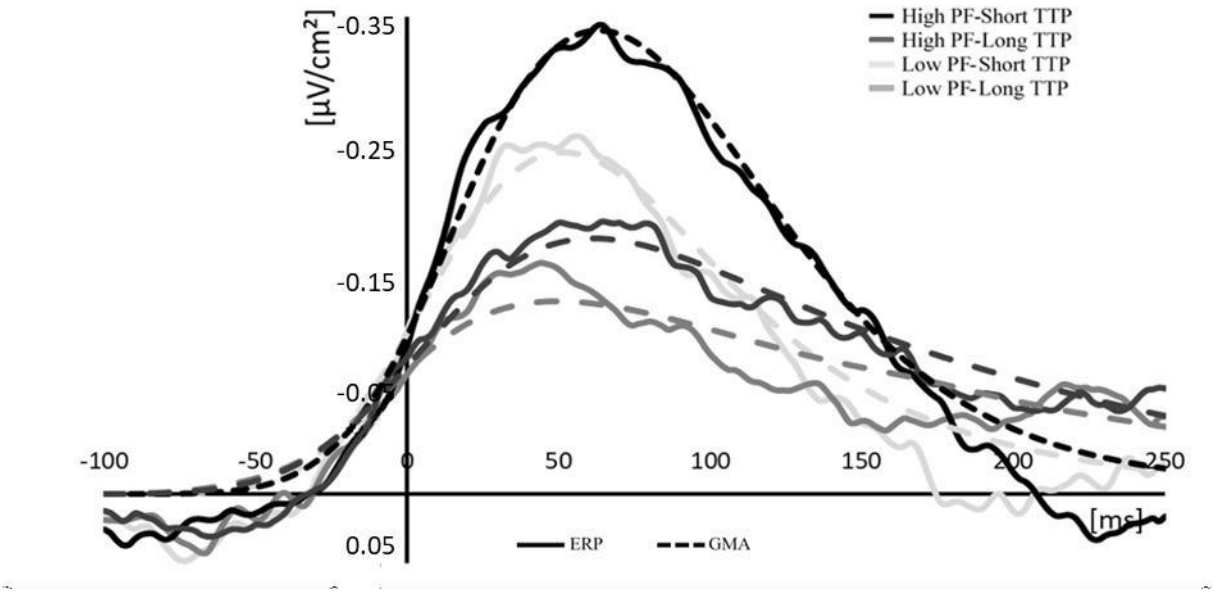

Figure 10. Grand average CSD-ERP waveforms at electrode site FCz and average of the gamma waveforms extracted from the model as a function of response type. Negative values are plotted upwards, and time point zero represents the response onset (Kummer et al., 2020).

6.2.2 Correlations between ERP parameters and GaM parameters

All significant correlation coefficients between the MFN latency and the GaM parameters are shown in Table 6. No significant correlations between two classical ERP parameters (peak amplitude, area) and the GaM parameters (time-dependent or shape-dependent) were found for any of the four conditions (for all correlation coefficients see Table A5, appendix).

Table 6. Overview of all significant correlation coefficients between the latency of the ERP component and the gamma model parameters of Study 4 (N = 18). Corrected for multiple comparisons through Šidák correction (all *p*s < .0006)

	GaM parameters	Latency
lowPF-shortTTP		
	Mode	.85
highPF-shortTTP		
	1st IP	.70
	Mode	.70
lowPF-longTTP		
	1st IP	.76
highPF-longTTP		
	1st IP	.83

Note: For all correlation coefficients, see Table A5, appendix.

This means that participants with an earlier Mode in the short-TTP condition showed a later latency. For the long-TTP condition, participants with a later latency showed a later first IP. A later first IP is also shown for participants with a later latency in the highPF-shortTTP condition.

6.2.3 Event-related potentials

In the next step, it is explored how well both methods – classical ERP analyses and GMA – could identify differences between experimental conditions (for means and *SD* for the classical parameters and the GaM parameters, see Table A6, and for all ANOVAs, see Table A7, appendix).

Classical analyses – peak. The ANOVA for peak amplitude showed that high force responses had a higher negative peak than low force responses, $F(1, 17) = 31.74$, $p < .001$, and a higher negative peak in the short TTP condition than in the long TTP condition, $F(1, 17) = 26.33$, $p < .001$. The two factors did not interact, $F(1, 17) = 2.85$, $p = .11$.

Classical analyses – area. The ANOVA of the component's first area revealed that high force responses had a larger area than low force responses, $F(1, 17) = 23.80$, $p < .001$, and that the area in the short TTP condition was larger than that in the long TTP condition, $F(1, 17) = 13.14$, $p = .002$. The Force Type x TTP Type interaction showed no significant effect, $F(1, 17) = 3.39$, $p = .08$.

Classical analyses – latency. The analysis of the MFN latency revealed no significant effects.

Gamma model analysis – time-dependent GaM parameters. There were no significant effects for the first IP and the mode. Although there were also no significant effects of Force Type or the Force Type x TTP Type interaction on the second IP (see Table A7), the ANOVA for the TTP Type revealed a significant effect on the second IP, $F(1, 17) = 7.12$, $p = .02$. Responses in the long TTP conditions had a significantly later second IP than responses in the short TTP conditions.

Gamma model analysis – shape-dependent GaM parameters. The ANOVAs of skewness and excess revealed neither a significant effect of Force Type nor a Force Type x TTP Type interaction. The TTP Type showed a significant effect on skewness, $F(1, 17) = 14.73$, $p = .001$. Responses with a longer TTP were significantly more skewed to the right than responses with a shorter TTP. There was also a significant effect of TTP Type on excess, $F(1, 17) = 13.57$, $p = .002$. Specifically, responses with a longer TTP had significantly thicker tails than responses with a shorter TTP. In summary, the gamma waveform of responses with a longer TTP was more skewed to the right and had heavier tails.

6.3 Discussion

The reanalysis identified the same effects on the ERP components as Armbrecht et al. (2013) reported (i.e. higher peak/larger first area for high force condition than for low force condition; a higher peak/larger area for short TTP condition than for long TTP condition, with the largest area for high force and short TTP responses). Very good overall fits between the empirical and the gamma waveforms indicated that the GMA was again very successful in fitting the component's shape. An effect of the TTP Type on the RMSEs was found, which might be due to a possible sign change occurring at the tail of the component for short TTP responses.

The main goal of this analysis was to examine whether experimentally induced variations of Response Force and TTP were reliably reflected in systematic variations in the shape of the fitted gamma waveform. While the Response Force showed no effects on GaM parameters (time-dependent and shape-dependent), the TTP Type affected three GaM parameters. This means that the Response Force had an effect on the peak amplitude of the ERP waveform, but it did not affect the timing and the overall shape. GMA components for responses with a long TTP also showed later second IPs; these responses were also more right-tailed and thicker-tailed than responses with a short TTP. These findings can be interpreted as longer monitoring for prolonged responses (i.e. force pulses with a long TTP), but this possibility has to be explored in more detail in future research.

Interestingly, as indicated by the non-significant correlation between two classical ERP parameters (peak amplitude, area) and the GaM parameters within the experimental conditions, these TTP Type relations with the GaM parameters appeared to be independent of any relations mirrored in these two classical ERP parameters. This suggests that the GaM parameters and the classical ERP parameters are not just two sides of the same coin; rather, the GMA seems to provide additional distinct information about the neural processes that are not captured by the ERP parameters.

7 Study 4: Flanker Task – Sign Change

As outlined previously, the gamma PDF is not able to fit a voltage-sign change, thus, the resulting fit of the GMA to the empirical ERP waveform is not perfect at the end of the time window. One might argue that the gamma PDF is therefore not the ideal function to fit ERP waveforms (Kummer et al., 2020). Since an ERP component can be defined as a “voltage change that reflects a specific neural or psychological process” (Kappenman & Luck, 2012, p. 2), this could reflect the beginning of a new component (most likely linked to a different cognitive process).

According to this definition, a specific voltage change could be described as a polarity-change or the point where the curvature of the ERP waveform changes its sign. These points where the waveform changes from an increasing slope (going upward) to a decreasing slope (going downward) or vice versa can be measured through IPs. GMA, however, specifically aims to describe and determine the parameters of only one component. Therefore, GMA only has to fit the ERP waveform until one of these specific voltage changes. Accordingly, the GMA does not have to fit a voltage-sign change if the second IP is before this change of polarity.

Subsequently, it was examined whether the second IPs are within the time-window of negative polarity and therefore before the voltage-sign change. Additionally, it was investigated whether the voltage-sign change has an influence on the resulting GaM parameters and the goodness-of-fit parameters from Studies 2 and 4 were compared. Thus, the sign-change should not affect the GaM parameters and the overall conclusion should be the same as in the previous study if the GMA only describes and models one component.

Therefore, the data from Study 2 was reanalysed, but with a flexible waveform length (see Material & Methods, section 4.1) at the end to avoid a voltage-sign change.

7.1 Material and methods

The participants, apparatus, procedure, and GMA are identical to Study 2.

7.1.1 Electrophysiological data

The EEG Recording and EEG pre-processing including the CSD transformation and segmentation are similar to Study 2. The flexible length for the ERP waveforms was attained through cropping each participant's averaged ERP waveforms separately for each response type, if a voltage-sign change from negative to positive occurred after response onset. The voltage-sign change had to be at least 50 ms long before the ERP waveform changed again from positive to negative. If this was the case, the ERP waveform was cropped from -100 ms to the time point of the voltage-sign change from negative to positive. Figure 11 shows an example of cropping an individual averaged waveform.

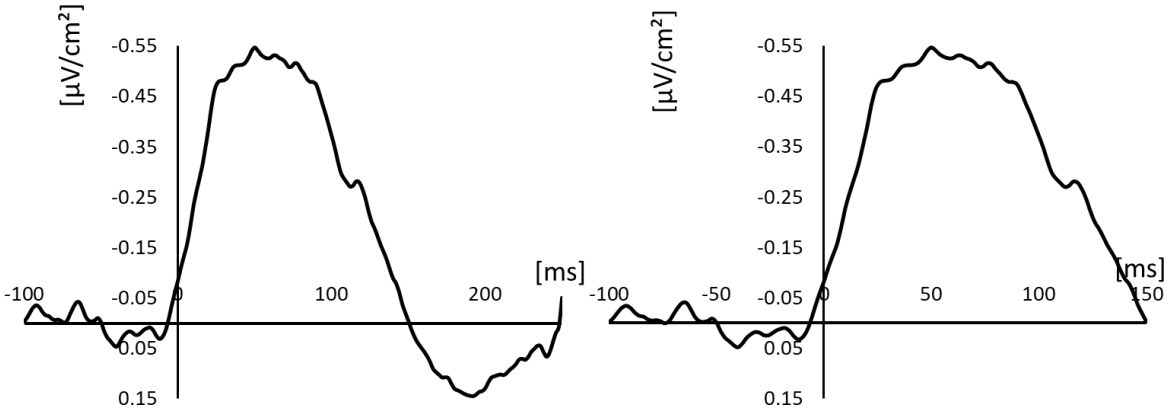

Figure 11. Two CSD-ERP waveforms at electrode site FCz as function of response type, (A) before cropping and (B) after cropping. Negative values are plotted upwards, and time point zero represents the response onset.

7.1.2 Gamma model analysis and statistical analyses

The GMA was performed identically to Section 3.3. The goodness-of-fit analyses were also identical to those of Study 2. For the polarity of the second IP, the current source density (µV/cm²) at corresponding IPs was measured. The frequency of a voltage-sign change was determined by measuring the point where ERP waveforms were cropped, as explained previously. Several *t*-tests were performed regarding response type (error vs correct) for the GaM parameters and regarding the goodness-of-fit parameters (Study 2 vs. Study 4). All statistical analyses were corrected for multiple comparisons using the Šidák correction (Šidák, 1967).

7.2 Results

7.2.1 Goodness-of-fit analysis

The individual correlations for erroneous responses ranged from $r = .63$ to $r = .99$ (mean $r = .95 \pm .39$) and from $r = .49$ to $r = .99$ (mean $r = .95 \pm .47$) for correct responses. The *t*-test showed no significant difference between the correlation coefficients for correct and erroneous responses, $t(112) = 1.94$, $p = .05$. The RMSE for erroneous responses ranged from RMSE = 0.012 to RMSE = 0.126 (mean RMSE = 0.036 ± 0.020) and from RMSE = 0.006 to RMSE = 0.117 (mean RMSE = 0.035 ± 0.02) for correct responses. The *t*-test showed no significant difference between the RMSEs for correct and erroneous responses, $t(112) = 0.60$, $p = .55$.

7.2.2 Polarity of the Second Inflection Point

The voltage of the second IP for erroneous responses ranged from -0.002 µV/cm² to -0.96 µV/cm² (mean: -0.22 ± 0.16 µV/cm²) and from -0.03 µV/cm² to -0.96 µV/cm² (mean: -0.24 ± 0.15 µV/cm²) for correct responses.

7.2.3 Event-Related Potentials

Several *t*-tests were conducted to examine the effect of the response type on each of the GaM parameters (Table 7). Correct responses had a larger rate parameter, a smaller shape parameter, and smaller scaling as erroneous responses as can be seen in Table 7. The analyses showed significant effects for two time-dependent parameters. Erroneous responses showed a later first IP and an earlier second IP compared to correct responses.

There was no significant effect for the mode parameter. For the shape-dependent parameters, the analysis showed that correct responses had a larger skewness and excess parameter compared to the erroneous responses.

Table 7. Mean, standard deviation (± SD), *t*-value, *p*-value and *r* for the gamma model parameters (shape parameter, rate parameter, scaling, first IP, second IP, mode, skewness, excess), separately for each response type (correct vs errors; N = 113). Corrected for multiple comparisons through Šidák correction.

Response Type	M	*t*	*p*	*r*
Basic Parameters				
Shape parameter				
Correct	20.86 ± 17.5	-3.77	< .006	.34
Error	27.20 ± 14.4			
Rate parameter				
Correct	0.26 ± 0.24	-3.65	< .006	.33
Error	0.33 ± 0.18			
Scaling				
Correct	1.32 ± 1.16			
Error	1.61 ± 0.90	3.09	< .006	.28
Time-Dependent Parameters				
First inflection point [ms]				
Correct	18.04 ± 21.6	-2.91	< .006	.27
Error	24.12 ± 13.2			
Mode [ms]				
Correct	65.35 ± 27.6	1.71	.09*	.16
Error	60.11 ± 24.0			
Second inflection point [ms]				
Correct	117.92 ± 51.3			
Error	98.85 ± 53.5	3.21	< .006	.29
Shape-Dependent Parameters				
Skewness				
Correct	0.53 ± 0.18	6.25	< .006	.51
Error	0.42 ± 0.13			
Excess				
Correct	0.47 ± 0.32	5.92	< .006	.45
Error	0.29 ± 0.22			

*non-significant: $p > .006$

The findings indicate that the ERP waveforms of erroneous responses had a later first IP, an earlier second IP, and were less skewed to the right, with thinner tails compared to correct responses.

7.2.4 Comparing goodness-of-fit parameters

Several *t*-tests were conducted to compare the goodness-of-fit parameters from Studies 2 and 4. The *t*-test revealed a significant difference between the correlation coefficients from Study 2 and Study 4 for correct responses, $t(112) = 5.23$, $p < .001$ and erroneous responses, $t(112) = 11.47$, $p < .001$, with higher correlation coefficients for Study 4 (correct: .95 ± .47; error: .95 ± .39) compared to Study 2 (correct: .92 ± .49; error: .90 ± .41).

Similarly, the *t*-test for the RMSEs exhibited a significant difference between Study 2 and Study 4 for correct responses, $t(112) = 3.30$, $p = .001$ and erroneous responses, $t(112) = 8.50$, $p < .001$, with smaller RMSEs for Study 4 (correct: 0.035 ± 0.020; error: 0.036 ± 0.020) compared to Study 2 (correct: 0.039 ± 0.020; error: 0.076 ± 0.056).

7.3 Discussion

The goal of Study 4 was to examine whether the GMA only describes and models one ERP component or whether it is influenced through specific voltage changes which could be the beginning of a new component. Therefore, the study examined if all second IPs ranging within a time-window with negative polarity and if the voltage-sign change at the end of the empirical ERP waveforms influences the resulting GaM parameters. The data from Study 2 was reanalysed with a flexible waveform length, which were cropped at an appropriate voltage-sign change at the end of the waveform.

The goodness-of-fit analyses still displayed high correlations between the gamma waveforms and ERP waveforms (on average, they explained 90% of the variance; R^2 ranged from 24% to 98%) and there was no significant difference between RMSEs for correct and erroneous responses. The GMA seemed to fit the observed waveforms very well. The significant differences between the RMSEs of correct and erroneous responses in Study 2 was not found in Study 4, which strengthens the argument that this difference in Study 2 occurred due to the sign change at the tail of the component.

Possible significant differences between the GaM parameters from Study 2 and Study 4 were not tested, because the flexible length of the empirical ERP waveforms lead to a different set of data for the GMA through the cropping procedure, which does not allow a comparison to be made between the two datasets.

The analysis of the second IPs in Study 4 showed that they are all ranging within a negative polarity of the ERP waveform and are therefore before a voltage-sign change. Further analyses identified the same sensitivity of the GaM parameters for the two investigated conditions. For two basic parameters, the time-dependent parameters and the shape-dependent parameters, significant effects were found. Hence, the results of Studies 2 and 4 lead to the same conclusion. Therefore, the voltage-sign change does not influence the resulting parameters crucially and the GMA fits all relevant parts of the given empirical ERP waveforms before a specific voltage change occurs.

Nevertheless, the calculated effect sizes *r* were higher in Study 2 and one might argue that Study 2 therefore showed better results using the uncropped ERP waveforms. However, since the GMA cannot model a voltage-sign change it performs an asymptotic approximation to the x-axis if the ERP waveform changes its polarity. This might have biased the model fit and led to an overestimation of the effect sizes in Study 2 through an unsatisfactory model. The significant better goodness-of-fit parameters in Study 4 support this impression that the size of the effect might not be the decisive parameter in this case.

These results lead to the conclusion that, if possible, it seems preferable to use cropped ERP waveforms for the GMA in future research.

8 Study 5: PDF Comparison

The GMA was successfully applied in the previous studies, as demonstrated by the results of the simulation study and the high correlations between the estimated gamma waveform and the empirical ERP waveforms. It explained up to 98% of the components' variance, independently of paradigm and behavioural manipulation. Nevertheless, there is the possibility that the application of other PDFs could show even better results regarding the goodness-of-fit analysis and consequently attain more precise shape-dependent and time-dependent parameters. Therefore, three additional PDFs (Weibull, Beta, Birnbaum-Saunders) were chosen to compare the respective goodness-of-fit parameters (RMSE, Pearson's correlation coefficient) with the results of the Gamma PDF for Study 4. The additional PDFs were all implemented in the algorithm of the GMA instead of the Gamma PDF.

8.1 Material and methods

The apparatus, participants, procedure, behavioural data, and electrophysiological data are identical to Study 4.

8.1.1 Model Analysis

The model analysis was performed identically to the previous study, except the Gamma PDF was replaced with three different PDFs which are briefly introduced.

Weibull PDF. The Weibull PDF is a commonly used distribution for survival analysis or failure data analysis and was chosen for this study because it has a similar shape compared to the Gamma PDF but is more platykurtic. This means it should show a better fit for distributions with thinner tails (Sagias & Karagiannidis, 2005; Weibull, 1951). A standard Weibull PDF is given by:

$$F(t) = \left\{ a\left(\frac{\beta}{\eta}\ \ \left(\frac{t}{\eta}\right)^{\beta-1} exp^{-\left(\frac{t}{\eta}\right)^{\beta}}\right) \qquad t \geq 0. \right. \tag{7}$$

with the *scale parameter* ($\eta > 0$), and *shape parameter* ($\beta > 0$) as functions of *time* ($t > 0$). Additionally, the function is scaled by a *scaling factor* ($a > 0$).

Beta PDF. The Beta PDF, also referred to as Pearson Type I distribution (Bagnoli & Bergstrom, 2005), was chosen because it is a well-known distribution and inter alia used in wavelet analysis (Kumar et al., 2012; Oliveira & Araújo, 2005). A standard Beta PDF is given by:

$$F(t) = \left\{ \eta \left(\frac{t^{a-1}(1-t)^{\beta-1}}{\mathrm{B}(a,\beta)} \right), where\ \mathrm{B(r,k)} = \frac{\Gamma(a)\Gamma(\beta)}{\Gamma(a+\beta)} \right. \quad (8)$$

with the *shape parameter* ($a > 0$), and *shape parameter* ($\beta > 0$) as functions of *time* ($t > 0$). Additionally, the function is scaled by a *scaling factor* ($\eta > 0$).

Birnbaum-Saunders PDF. The Birnbaum-Saunders PDF, which has a close relationship to the normal distribution, was developed as a new two-parameter parametric distribution for fatigue studies in material science (Birnbaum & Saunders, 1969). The Birnbaum-Saunders PDF was chosen because it is described as a “highly flexible lifetime model that admits different degrees of kurtosis and asymmetry” (Sanhueza et al., 2008, S. 646). Additionally, it is supported that this PDF should be used for distributions with moderate or large excess and skewness (Genç, 2013). The Birnbaum-Saunders PDF is given by:

$$F(t) = \left\{ a \left(\frac{1}{2\beta^2\gamma^2\sqrt{\Pi}} \left(\frac{t^2-\beta^2}{\sqrt{\frac{t}{\beta}} - \sqrt{\frac{\beta}{t}}} \right) exp^{\left(-\frac{1}{\gamma^2}\left(\frac{t}{\beta} + \frac{\beta}{t} - 2 \right) \right)} \right) \right. \quad (9)$$

with the *scale parameter* ($\beta > 0$), and *shape parameter* ($\gamma > 0$) as functions of *time* ($t > 0$). Additionally, the function is scaled by a *scaling factor* ($\alpha > 0$).

8.1.2 Statistical analysis

Goodness-of-fit analyses were performed for all used PDFs (see Study 2). Two-way analyses of variance (ANOVAs) with the within-subject factors Response Type (error vs. correct) and PDF Type (Gamma vs. Beta vs. Weibull vs. Birnbaum-Saunders) for the within-subject RMSEs. Furthermore, correlation coefficients were performed to compare the goodness-of-fit for the different PDFs. The reported correlation coefficients are Pearson's correlations (correlations including Fisher's *z*-standardised before averaging). Within-subject effects were analysed using Tukey's HSD post hoc tests.

8.2 Results

Table 8 shows the mean, standard deviation, and range for all correlations and RMSEs of the goodness-of-fit analyses of the ERP waveforms and the PDFs used (Figure 12).

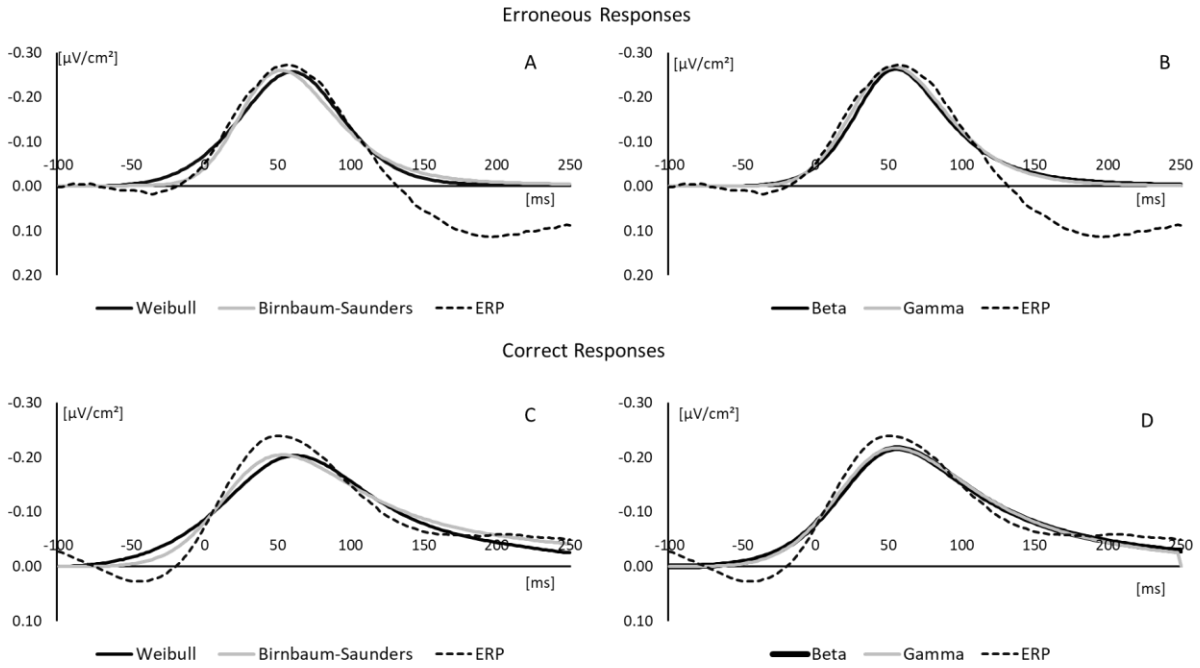

Figure 12. Grand average CSD-ERP waveform at electrode site FCz and averaged gamma waveforms for erroneous and correct responses extracted from the model fit. (A) Weibull PDF, Birnbaum-Saunders PDF, and ERP waveform for erroneous responses. (B) Beta PDF, Gamma PDF, and ERP waveform for erroneous responses. (C) Weibull PDF, Birnbaum-Saunders PDF, and ERP waveform for correct responses. (D) Beta PDF, Gamma PDF, and ERP waveform for correct responses. Negative values are plotted upwards and time point zero represents the response onset.

The ANOVA for Pearson's correlations showed that erroneous responses (.94 ± .46) had a higher correlation coefficient than correct responses (.92 ± .52), $F(1, 121) = 12.65$, $p < .001$. There was also a significant effect for PDF Type, $F(1, 121) = 5.83$, $p < .001$. Post-hoc tests indicated that the correlation coefficient for the Gamma PDF (.94 ± .47) was significantly higher compared to the Weibull PDF (.92 ± 50) and Birnbaum-Saunders PDF (.92 ± .56), while the test showed no significant differences between the Beta PDF (.93 ± .44) and the other three PDFs. The interaction between the Response Type and PDF Type also showed a significant effect, $F(1, 121) = 7.031$, $p < .001$. Post-hoc tests for correct responses revealed the Gamma PDF, Beta PDF, and Birnbaum-Saunders PDF had significantly higher correlation coefficients compared to the Weibull PDF. For the erroneous responses, the post-hoc tests showed that the Birnbaum-Saunders PDF had a significantly lower correlation coefficient than the Gamma PDF and the Weibull PDF.

Table 8. Mean, standard deviation (± *SD*) and range for Pearson's correlation coefficients and root mean square errors for the goodness-of-fit analyses comparing the estimated PDF waveforms (Gamma, Weibull, Beta, Birnbaum-Saunders) with the observed ERP waveforms for both Response Types (error vs correct; N = 18)

	Pearson's correlation		*Root mean square errors*	
	mean	range	mean	range
Erroneous Responses				
Gamma	.95 ± .41	.51 to .99	0.037 ± 0.021	0.012 to 0.126
Weibull	.95 ± .48	.12 to .99	0.036 ± 0.020	0.011 to 0.115
Beta	.94 ± .41	.47 to .99	0.037 ± 0.019	0.011 to 0.124
Birnbaum	.92 ± .53	.25 to .99	0.041 ± 0.021	0.011 to 0.121
Correct Responses				
Gamma	.93 ± .52	.49 to .99	0.035 ± 0.018	0.006 to 0.084
Weibull	.89 ± .51	.08 to .99	0.042 ± 0.022	0.008 to 0.111
Beta	.92 ± .48	.10 to .99	0.039 ± 0.037	0.008 to 0.343
Birnbaum	.92 ± .58	.10 to .99	0.037 ± 0.019	0.007 to 0.114

The ANOVA for RMSEs showed neither a significant effect for the Response Type, $F(1, 121) = 0.160$, $p = .69$, nor for the PDF Type, $F(1, 121) = 1.48$, $p = .22$. The interaction between Response Type and PDF Type revealed a significant effect, $F(1, 121) = 3.50$, $p < .02$. Post-hoc tests revealed that the Gamma PDF showed a smaller RMSE compared to the Weibull PDF for correct responses.

8.3 Discussion

Study 5 examined if a PDF other than the commonly used Gamma PDF could obtain a better fit to the empirical ERP waveforms by using the introduced model fit analysis. Three different PDFs (Weibull, Beta, Birnbaum-Saunders) were chosen and implemented in the previously used grid restrained nelder-mead algorithm to compare the respective goodness-of-fit parameters (RMSE, Pearson's correlation coefficient). Finally, the resulting goodness-of-fit parameters were compared with the findings from Study 4.

The goodness-of-fit analysis for the three implemented PDFs all displayed fairly good results. The statistical analysis showed no significant differences between the Gamma PDF and Beta PDF, for the RMSEs, nor for the correlation coefficients.

However, for the RMSEs the analysis identified one significant difference between the Gamma PDF and the Weibull PDF for correct responses. For the correlation coefficients there were several significant differences. First, the Weibull PDF definitively obtained the lowest correlation coefficient for the correct responses compared to the other three PDFs. Second, the Birnbaum-Saunders showed the lowest correlation coefficient regarding erroneous responses compared to the three other PDFs.

These results can be explained by looking at the properties of the PDFs and the empirical ERP waveforms. As shown in Study 2 and Study 4, the ERP waveforms for correct responses were more skewed to the right with thicker tails, which means they had higher skewness and excess parameters. Since the Weibull PDF is more platykurtic and therefore has thinner tails (Sagias & Karagiannidis, 2005), it had difficulties in achieving a good fit regarding the correct responses. On the other hand, the Birnbaum-Saunders PDF should be used for distributions with moderate to large excess and skewness (Genç, 2013). Thus, the Birnbaum-Saunders PDF attained good results regarding the right-skewed and thicker-tailed waveforms of the correct responses, but had trouble fitting the erroneous responses with smaller excess and skewness parameters.

As a result, the Gamma PDF and Beta PDF showed the best results for the goodness-of-fit analysis and seemed to preferably handle the different skewness and tailedness of the empirical ERP waveforms in this study. Consequently, the Gamma PDF can be maintained for the introduced model analysis, because none of the three additional implemented PDFs showed better results.

Nevertheless, the results also suggest that model fit depends on the distribution of the empirical ERP waveform. This study included only the MFN and it could be that, for example, the Birnbaum-Saunders PDF might show a better model fit analysing the waveform of the P3 because of its properties. One line of future research could therefore be the investigation of different PDFs for different ERP components.

9 General Discussion

The goal of this thesis was to introduce the GMA as a new method to analyse ERP data. The reason for developing an additional scoring method was that the commonly applied scoring methods, namely peak, area, and latency measures, were unable to analyse the essential variations in size and shape across individual ERP waveforms, besides all their aforementioned weaknesses. Thus, significant information from ERP waveforms was frequently missed out. This information could indicate neuroanatomical variations or reflect differences in processing related to specific personality and behavioural variables, among others (Kappenman & Luck, 2012; Luck, 2014). Supplementary to the classical scoring methods (peak, area, and latency), the GMA therefore enables the analysis of specific shape-related and different time-related information regarding an ERP component through statistical testing of changes in the resulting GaM parameters (Kummer et al., 2020).

The GMA was evaluated in a simulation study (Study 1), in which the reliability and validity of the method was examined by applying the GMA to simulated noisy ERPs with an induced effect. The results showed that the GMA was able to identify this induced effect and that there was neither systematic overestimation nor a systematic underestimation due to the generated noise.

Subsequently, data of a digit flanker task (Study 2) and from a force production task (Study 3) were reanalysed to investigate whether the GMA was an appropriate method to fit empirical data and if the GaM parameters were sensitive to experimentally induced variations. Regardless of the limitation that the gamma PDF is not able to perform a voltage-sign change, the GMA showed a very good model fit to the observed waveforms in Study 2 and Study 3.

Additionally, the results of both studies indicate that the GMA provides an additional set of interpretable parameters with unique information about the neural process, like the rise and decline of a component's waveform, which are not captured by the classical ERP parameters (Kummer et al., 2020).

Thereafter, the data from Study 3 was used to investigate the inability of the Gamma PDF to model a voltage-sign change as a potential limitation (Study 4). The results signified that there is no crucial influence on the resulting GaM parameters through a voltage-sign change and that the GMA is able to fit all essential parts of the given empirical ERP waveforms. After showing that PDFs are able to fit empirical ERP waveforms successfully, Study 5 eventually examined if other PDFs revealed better results regarding the goodness-of-fit parameters compared to the chosen Gamma PDF. Three different PDFs (Weibull, Beta, Birnbaum-Saunders) were implemented in the algorithm previously used for the GMA instead of the Gamma PDF. In this study, the Gamma PDF and Beta PDF showed the best goodness-of-fit parameters, since the Gamma PDF and the Beta PDF seem to be substantially more flexible than the Weibull PDF and the Birnbaum-Saunders PDF regarding the shape of the examined ERP waveforms.

9.1 Why use the gamma PDF?

The Gamma PDF was used as a mathematical function, since it had been applied successfully to comparable EEG data in a previous study (Stahl, 2010). The typical characteristics of most ERP waveforms are a prompt rise and a slow decline, which is also a feature of the Gamma PDF. However, as mentioned previously the GMA is not able to fit the positive component following the MFN, as PDFs in general cannot model a voltage-sign change. This can be seen in the reduced fits at the tail end of the component due to an asymptotic approximation to the x-axis. This might raise the question of whether PDFs are the right functions to fit ERP waveforms. Indeed, it might arguably be better to model a voltage-sign change or rather the transition between the neural processes with more complex functions (e.g. polynomials). A major disadvantage of using polynomials, however, would be that an individual equation must be created for every single ERP waveform of interest. Furthermore, the polynomial had to be at least cubic, and correspondingly it would clearly be more complex to obtain shape-dependent parameters and time-dependent parameters, like the GMA does.

In case of the IPs, for example, the second derivate would have to be computed separately for every waveform. In contrast, PDFs are relatively simple functions, which can be computed much easier; as such, one PDF can be used for all ERP waveforms of interest. Additionally, the interpretation and calculation of the parameters in PDFs is straightforward and uncomplicated. The significantly better goodness-of-fit parameters even lead to the conclusion that it might be preferable to use cropped ERP waveforms for the GMA in future research. Ultimately, the goal of GMA is to analyse ERPs and not voltage-sign changes (Kummer et al., 2020). Along with the results from Study 5, which showed that no investigated PDF had better goodness-of-fit than the Gamma PDF, it can be summarised that the Gamma PDF should be kept for the introduced model analysis.

9.2 Outlier analysis

The number of dropouts (Study 2: n = 8 out of 121; Study 3: n = 3 out of 24) due to an inappropriate mode-peak match or the RMSE-based outlier test may be perceived as a disadvantage of GMA. On the one hand, the method might neglect important effects that would be reflected in the data when using the classical scoring methods, especially in studies with a small sample. On the other hand, if the GMA is not capable of fitting a component for an individual, this could suggest that the individual's component has no clear shape. This might be due to high levels of noise or the absence of a solid, reproducible ERP component. Indeed, visual inspection of the ERPs in the studies with unsuccessful model fits supports the latter assumption (Figure 13). Therefore, rather than being a limitation of the method, unsuccessful model fits might help to identify ill-described individual components and could provide a reasonable basis for excluding participants who would otherwise add noise to the analyses. Unlike classical analyses, which would rely on visual inspection, GMA has the benefit of being a mathematical procedure, thus allowing for an objective and automated exclusion approach. Of course, future studies are required to investigate systematic variations in dropouts (e.g. with experimental conditions, or individual characteristics such as RT, personality scores, etc.). No indication of such systematic variation was found in the present studies.

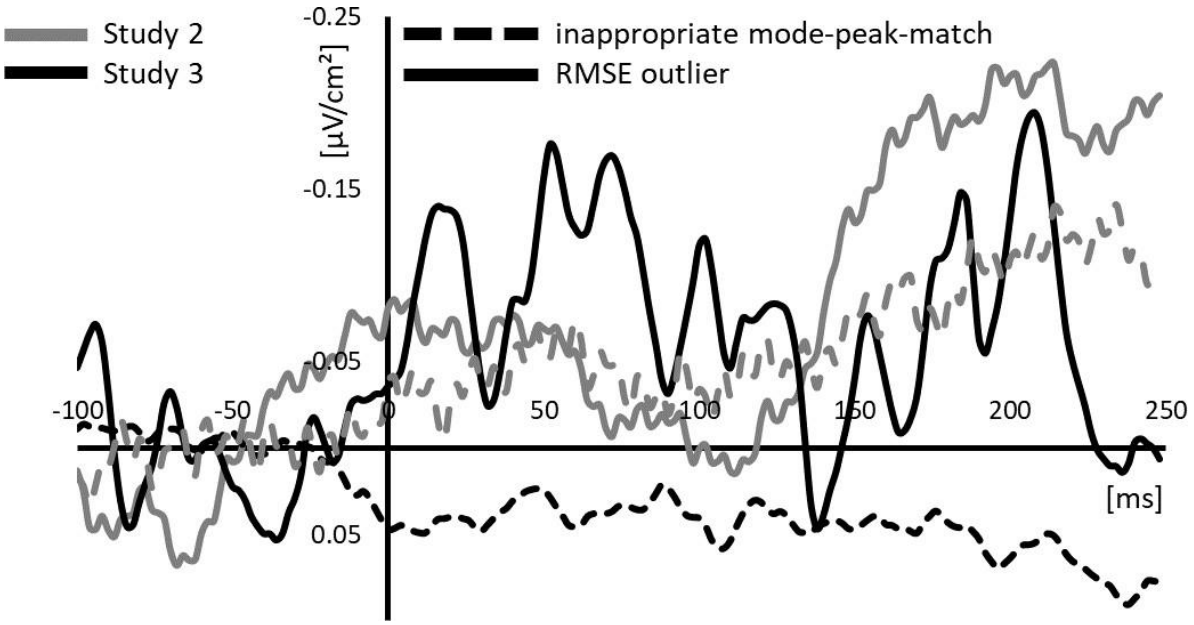

Figure 13. Examples of individual CSD-ERP waveforms at electrode site FCz for the RMSE outliers and the inappropriate mode-peak match for both studies. Negative values are plotted upwards and time point zero represents the response onset. The identified individuals did not show waveforms that could be described as the ERN/Ne in a meaningful way.

9.3 Meaning of the gamma model parameters

Information about the time course of the waveform is given by three time-dependent parameters: the first IP, the mode, and the second IP. Information about the shape of a waveform is given by the two shape parameters, skewness, and excess.

9.3.1 Additional temporal information of the neural process.

In Study 3 and Study 4, significant correlations between the three time-dependent parameters (first IP, mode, second IP) and the peak latency were found, showing that the temporal dynamics of a neural process are not independent. As demonstrated by the significant response type effect (erroneous vs. correct response) on the time-dependent GaM parameters in the first empirical study, however, these parameters revealed additional information about the ERP component which were not reflected by the peak latency. Specifically, correct responses had an earlier first IP and later second IP compared to erroneous responses. A similar effect was not present in the latency parameter, though.

By considering the time-dependent GaM parameters, it is possible to differentiate between temporal aspects of an ERP waveform. Moreover, the first IP and second IP also contained further information, respectively. The second IP, but not the first IP, was sensitive to TTP Type variations in the second study. In the long TTP condition, compared to the short TTP condition, a significantly later second IP was found. Assuming that a longer TTP requires longer action monitoring (Armbrecht et al., 2013), a later second IP presumably reflects a longer duration of neuronal processing.

Although no effect on the first IP was revealed, it is reasonable to assume that an effect could be found for some paradigms in which the onset of neural processes is expected to vary. This is due to more or less available information per time unit, or because of individual variations (e.g. the neural efficiency hypothesis of intelligence, Neubauer & Fink, 2009). Temporal predictions could be tested using the first IP as a measure.

9.3.2 Additional shape information of the neural process.

The two shape parameters — skewness and excess — are mathematically related terms (see Equations 3 and 4). A positive skewness means that the waveform is skewed to the right. The excess parameter relates to how heavy tailed an ERP waveform is. A positive excess means that the waveform has heavier and longer tails. Higher positive skewness and excess parameters thus indicate that the ERP waveform is more skewed to the right and has a longer right tail. Considering the two IPs with regard to skewness and excess, it is also possible to learn more about the component's rise and decline (for the parameters' relationships see Equations 5 and 6). This information might help, as described above, to test hypotheses about the variation of neuronal accumulation during action monitoring (e.g. Bode & Stahl, 2014) and how this might vary between experimental conditions.

9.3.3 Interdependence of the GaM parameters

It is important to bear in mind that, while different parameters shed light on separate features of the component (and therefore relate to different aspects of the cognitive process of interest), the interdependence of the GaM parameters also always require the findings to be interpreted more holistically. This is demonstrated in the following example: the fitted GMA waveforms in the long TTP condition compared to the short TTP condition (Study 3) showed no difference in the first IP, but they were more skewed to the right, had a later second IP and heavier tails. This means that the ERP for the longer TTP had a similar rise but a slower decline of neural activity.

An interpretation of this may be that the two processes start similarly, but then a longer TTP requires longer and sustained ongoing neuronal processing than a shorter TTP (see Armbrecht et al., 2013). The full picture here does not emerge from the interpretation of single parameters but from their integration.

9.4 Limitations of the approach and future research

A possible limitation of the GMA is the number of parameters which the method produces. This could give the impression that GMA is just another way to search for significance in experimental data, also known as '*p* hacking' (e.g. Head et al., 2015; Ioannidis, 2005) Nevertheless, different methods that produce several parameters can make the same impression. One crucial advantage of the GMA's supply of data, though, is that researchers can make transparent and exact predictions in advance to test their models and theories (for example, testing Armbrecht et al.'s mathematical model of force unit monitoring; Armbrecht et al., 2013; Kummer et al., 2020).

The GMA requires further exploratory studies to understand the reaction and significance of the GaM parameters to different experimental variations. For example, a later second IP and a more right-skewed waveform in Study 3 could indeed imply a longer action monitoring process. By contrast, a prolonged response in this task might lead to the activation of a different set of neurons than in a short response. Accordingly, the measured variation in the ERP waveform could also be attributed to the underlying cortical folding and not be a temporal aspect (Kappenman & Luck, 2012; Kropotov, 2009; Luck, 2014).

Nonetheless, Bishop et al. (2007) wrote that they require methods to detect neurobiological abnormalities in auditory ERPs to research developmental language disorders. The GMA might thus be an additional method to discover relevant neurobiological differences in the auditory ERP waveforms, which the classical methods might neglect.

Besides the possible neuroanatomical variations, the research field could benefit from GMA with regards to the detection of individual differences. Luck (2014) proposed the idea that variation in the ERP waveform could also reflect personality-related variations. For instance, the GMA might detect previously unknown shape-related or time-related differences in ERP waveforms regarding different personality traits (e.g. perfectionism, narcissism, neuroticism; Kummer et al., 2020).

The GMA could also lead to new insights regarding the effect of behavioural variations on ERPs. For example, covert incorrect response, so-called partial errors, might not only influence the MFN amplitude but also lead to shape-related differences in the ERP waveform. This might help to gain further insights into the contradictory findings of decreased MFN amplitudes for partial errors compared to so-called full errors (Endrass et al., 2008; Masaki & Segalowitz, 2004), and same-sized MFN amplitudes for partial errors and full errors (Carbonnell & Falkenstein, 2006; Scheffers et al., 1996).

Furthermore, the GMA might also be used as an approximation to measure the onset or offset latency of an ERP component; this might be more useful in the testing of various neurocognitive or affective theories than the usual method of measuring the process timing (the peak latency). As already pointed out, the peak latency is the time-point of the maximum amplitude and therefore not necessarily sensitive to an actual temporal shift, nor the starting time or ending time of an ERP component (Kiesel et al., 2008; Luck, 2014).

However, there are some promising techniques to evaluate the onset latencies of ERP components like the fractional area technique (Luck, 2014), the fractional peak latency (Luck, 2014), and the jackknife approach (Stahl & Gibbons, 2004; Ulrich & Miller, 2001). However, these methods also have their limitations, since researchers must still consider the visual appearance of the ERP waveform and have to handle rough recommendations on how to use these methods (Kiesel et al., 2008).

The GMA might provide supplementary information about the time-course of an ERP component without being affected by these limitations, as it is possible to calculate the point in time where the modelled gamma waveform shows a substantial deviation from zero, both at the start and the ending. Future simulation studies using the GMA to measure the onset and offset latencies of ERP waveforms can provide further insights into whether the GMA is an appropriate technique in these cases.

Finally, a further benefit of the GMA is that the method could be more directly integrated into mathematical modelling compared to the classical ERP analyses, since the method facilitates a mathematical description of ERP components (for a discussion on the benefit of mathematical models in neuroscience, see Ulrich, 2009).

9.5 Conclusion

GMA is a novel approach to the investigation of ERP components' shape, here demonstrated for the MFN (and simulated data). The different GaM parameters were sensitive to various experimental manipulations across the empirical studies. Moreover, the GMA revealed several additional interrelated but non-redundant parameters compared to the classical methods (peak amplitude, area measurement), which were predictive of different aspects of behaviour, allowing for a more nuanced analysis of the cognitive processes. GMA provides an elegant method for extracting easily interpretable indices for the rise and decline of the components that complement the classical parameters. This can be beneficial in gaining a better understanding of the neural mechanisms that underlie cognitive processes.

10 References

Allain, S., Carbonnell, L., Burle, B., Hasbroucq, T. & Vidal, F. (2004). On-line executive control: An electromyographic study. *Psychophysiology*, *41*(1), 113–116. https://doi.org/10.1111/j.1469-8986.2003.00136.x

Armbrecht, A.-S., Gibbons, H. & Stahl, J. (2012). Monitoring force errors: Medial- frontal negativity in a unimanual force-production task. *Psychophysiology*, *49*(1), 56–72. https://doi.org/10.1111/j.1469-8986.2011.01282.x

Armbrecht, A.-S., Gibbons, H. & Stahl, J. (2013). Effects of Response Force Parameters on Medial-Frontal Negativity. *PLoS ONE*, *8*(1), e54681. https://doi.org/10.1371/journal.pone.0054681

Bagnoli, M. & Bergstrom, T. (2005). Log-concave probability and its applications. *Economic Theory*, *26*(2), 445–469. https://doi.org/10.1007/s00199-004-0514-4

Barnston, A. G. (1992). Correspondence among the Correlation, RMSE, and Heidke Forecast Verification Measures; Refinement of the Heidke Score. *Weather and Forecasting*, *7*(4), 699–709. https://doi.org/10.1175/1520- 0434(1992)007<0699:CATCRA>2.0.CO;2

Baudin, M. (2010). *Nelder-Mead User's Manual*. Consortium Scilab - Digiteo. Berger, H.

(1931). Über das Elektrenkephalogramm des Menschen. *Archiv für Psychiatrie und Nervenkrankheiten*, *94*(1), 16–60. https://doi.org/10.1007/BF01835097

Bernstein, P. S., Scheffers, M. K. & Coles, M. G. H. (1995). "Where did I go wrong? " A psychophysiological analysis of error detection. *Journal of Experimental Psychology: Human Perception and Performance*, *21*(6), 1312–1322. https://doi.org/10.1037/0096-1523.21.6.1312

Birbaumer, N. & Schmidt, R. F. (2010). *Biologische Psychologie*. Springer Berlin Heidelberg. https://doi.org/10.1007/978-3-540-95938-0

Birnbaum, Z. W. & Saunders, S. C. (1969). A new family of life distributions. *Journal of Applied Probability*, *6*(2), 319–327. https://doi.org/10.2307/3212003

Bishop, D. V. M., Hardiman, M., Uwer, R. & Suchodoletz, W. von (2007). Atypical long-latency auditory event-related potentials in a subset of children with specific language impairment. *Developmental science*, *10*(5), 576–587. https://doi.org/10.1111/j.1467-7687.2007.00620.x

Bode, S. & Stahl, J. (2014). Predicting errors from patterns of event-related potentials preceding an overt response. *Biological Psychology*, *103*, 357–369. https://doi.org/10.1016/j.biopsycho.2014.10.002

Bonnar, J. (2014). *The Gamma function* (Third edition). Applied Research Press. Botvinick, M.

M., Braver, T. S., Barch, D. M., Carter, C. S. & Cohen, J. D. (2001). Conflict monitoring and cognitive control. *Psychological Review*, *108*(3), 624–652. https://doi.org/10.1037/0033-295X.108.3.624

Boutros, N. (2011). Historical Review of Electroencephalography in Psychiatry. In N. Boutros, S. Galderisi, O. Pogarell & S. Riggio (Hg.), *Standard Electroencephalography in Clinical Psychiatry* (S. 1–6). John Wiley & Sons, Ltd.

Bruijn, E. R. A. de, Hulstijn, W., Meulenbroek, R. G. J. & van Galen, G. P. (2003). Action monitoring in motor control: ERPs following selection and execution errors in a force production task. *Psychophysiology*, *40*(5), 786–795. https://doi.org/10.1111/1469-8986.00079

Bucci, P. & Galderisis, S. (2011). Physiologic Basis of the EEG Signal. In N. Boutros, S. Galderisi, O. Pogarell & S. Riggio (Hg.), *Standard Electroencephalography in Clinical Psychiatry* (S. 7–12). John Wiley & Sons, Ltd.

Burle, B., Possamaï, C.-A., Vidal, F., Bonnet, M. & Hasbroucq, T. (2002). Executive control in the Simon effect: An electromyographic and distributional analysis. *Psychological research*, *66*(4), 324–336. https://doi.org/10.1007/s00426-002-0105-6

Bűrmen, Á., Puhan, J. & Tuma, T. (2006). Grid Restrained Nelder-Mead Algorithm. *Computational Optimization and Applications*, *34*(3), 359–375. https://doi.org/10.1007/s10589-005-3912-z

Carbonnell, L. & Falkenstein, M. (2006). Does the error negativity reflect the degree of response conflict? *Brain research*, *1095*(1), 124–130. https://doi.org/10.1016/j.brainres.2006.04.004

Carter, C. S., Braver, T. S., Barch, D. M., Botvinick, M. M., Noll, D. & Cohen, J. D. (1998). Anterior cingulate cortex, error detection, and the online monitoring of performance. *Science (New York, N.Y.)*, *280*(5364), 747–749.

Clayson, P. E., Baldwin, S. A. & Larson, M. J. (2013). How does noise affect amplitude and latency measurement of event-related potentials (ERPs)? A methodological critique and simulation study. *Psychophysiology*, *50*(2), 174–186. https://doi.org/10.1111/psyp.12001

Coles, M. G. H. & Rugg, M. D. (2002). Event-related brain potentials: An introduction. In M. D. Rugg (Hg.), *Oxford psychology series: Bd. 25. Electrophysiology of mind: Event-related brain potentials and cognition* (S. 1–26). Oxford Univ. Press. https://doi.org/10.1093/acprof:oso/9780198524168.003.0001

David, O., Kiebel, S. J., Harrison, L. M., Mattout, J., Kilner, J. M. & Friston, K. J. (2006). Dynamic causal modeling of evoked responses in EEG and MEG. *NeuroImage*, *30*(4), 1255–1272. https://doi.org/10.1016/j.neuroimage.2005.10.045

Dochin, E., Ritter, W. & McCallum, W. C. (1978). Cognitive psychophysiology: The endogenous components of the ERP. *Event-related brain potentials in man*, *349*, 411.

Donchin, E. & Heffley, E. F. (1978). Multivariate analysis of event-related potential data: A tutorial review. In D. Otto (Hg.), *Multidisciplinary Perspectives in Event- Related Brain Potential Research* (S. 555–572). U.S. Government Printing Office.

Endrass, T., Klawohn, J., Schuster, F. & Kathmann, N. (2008). Overactive performance monitoring in obsessive-compulsive disorder: ERP evidence from correct and erroneous reactions. *Neuropsychologia*, *46*(7), 1877–1887. https://doi.org/10.1016/j.neuropsychologia.2007.12.001

Falkenstein, M., Hohnsbein, J., Hoormann, J. & Blanke, L. (1991). Effects of crossmodal divided attention on late ERP components. II. Error processing in choice reaction tasks. *Electroencephalography and Clinical Neurophysiology*, *78*(6), 447–455. https://doi.org/10.1016/0013-4694(91)90062-9

Forster, B. & Pavone, E. F. (2008). Electrophysiological correlates of crossmodal visual distractor congruency effects: Evidence for response conflict. *Cognitive, Affective, & Behavioral Neuroscience*, *8*(1), 65–73. https://doi.org/10.3758/CABN.8.1.65

Gehring, W. J. & Knight, R. T. (2000). Prefrontal-cingulate interactions in action monitoring. *Nature neuroscience*, *3*(5), 516–520. https://doi.org/10.1038/74899

Gehring, W. J., Liu, Y., Orr, J. M. & Carp, J. (2012). The Error-Related Negativity (ERN/Ne). In S. J. Luck & E. S. Kappenman (Hg.), *Oxford library of psychology. The Oxford handbook of event-related potential components.* Oxford Univ. Press.

Gehring, W. J., Goss, B., Coles, M. G. H., Meyer, D. E. & Donchin, E. (1993). A Neural System for Error Detection and Compensation. *Psychological Science*, *4*(6), 385–390.

Gehring, W. J. & Willoughby, A. R. (2002). The medial frontal cortex and the rapid processing of monetary gains and losses. *Science (New York, N.Y.)*, *295*(5563), 2279–2282. https://doi.org/10.1126/science.1066893

Genç, A. İ. (2013). The generalized T Birnbaum–Saunders family. *Statistics*, *47*(3), 613–625. https://doi.org/10.1080/02331888.2011.628021

Gibbons, H., Fritzsche, A.-S., Bienert, S., Armbrecht, A.-S. & Stahl, J. (2011). Percept-based and object-based error processing: An experimental dissociation of error-related negativity and error positivity. *Clinical Neurophysiology*, *122*(2), 299– 310. https://doi.org/10.1016/j.clinph.2010.06.031

Gratton, G., Coles, M. G.H. & Donchin, E. (1983). A new method for off-line removal of ocular artifact. *Electroencephalography and Clinical Neurophysiology*, *55*(4), 468–484. https://doi.org/10.1016/0013-4694(83)90135-9

Gratton, G., Kramer, A. F., Coles, M. G.H. & Donchin, E. (1989). Simulation Studies of Latency Measures of Components of the Event-Related Brain Potential. *Psychophysiology*, *26*(2), 233–248. https://doi.org/10.1111/j.1469-8986.1989.tb03161.x

Head, M. L., Holman, L., Lanfear, R., Kahn, A. T. & Jennions, M. D. (2015). The extent and consequences of p-hacking in science. *PLoS biology*, *13*(3), e1002106. https://doi.org/10.1371/journal.pbio.1002106

Holroyd, C. B. & Coles, M. G. H. (2002). The neural basis of human error processing: Reinforcement learning, dopamine, and the error-related negativity. *Psychological Review*, *109*(4), 679–709. https://doi.org/10.1037/0033-295X.109.4.679

Hoormann, J., Falkenstein, M., Schwarzenau, P. & Hohnsbein, J. (1998). Methods for the quantification and statistical testing of ERP differences across conditions. *Behavior Research Methods, Instruments, & Computers*, *30*(1), 103–109.

Ioannidis, J. P. A. (2005). Why most published research findings are false. *PLoS medicine*, *2*(8), e124. https://doi.org/10.1371/journal.pmed.0020124

Kamel, N. & Malik, A. S. (Hg.). (2015). *EEG/ERP analysis: Methods and applications*. CRC Press Taylor & Francis Group.

Kappenman, E. S. & Luck, S. J. (2012). ERP Components: The Ups and Downs of Brainwave Recordings. In S. J. Luck & E. S. Kappenman (Hg.), *Oxford library of psychology. The Oxford handbook of event-related potential components* (S. 3– 30). Oxford Univ. Press.

Keil, A., Debener, S., Gratton, G., Junghöfer, M., Kappenman, E. S., Luck, S. J., Luu, P., Miller, G. A. & Yee, C. M. (2014). Committee report: Publication guidelines and recommendations for studies using electroencephalography and magnetoencephalography. *Psychophysiology*, *51*(1), 1–21. https://doi.org/10.1111/psyp.12147

Kiebel, S. J., David, O. & Friston, K. J. (2006). Dynamic causal modelling of evoked responses in EEG/MEG with lead field parameterization. *NeuroImage*, *30*(4), 1273–1284. https://doi.org/10.1016/j.neuroimage.2005.12.055

Kiesel, A., Miller, J., Jolicoeur, P. & Brisson, B. (2008). Measurement of ERP latency differences: A comparison of single-participant and jackknife-based scoring methods. *Psychophysiology*, *45*(2), 250–274. https://doi.org/10.1111/j.1469- 8986.2007.00618.x

Krishnamoorthy, K. (2016). *Handbook of statistical distributions with applications* (Second edition). CRC Press. http://search.ebscohost.com/login.aspx?direct=true&scope=site&db=nlebk&AN=1087849

Kropotov, I. D. (2009). *Quantitative EEG, event-related potentials and neurotherapy* (1st ed.). Elsevier/Academic. http://site.ebrary.com/lib/alltitles/docDetail.action?docID=10254769

Kumar, R., Kumar, A. & Pandey, R. K. (2012). Electrocardiogram Signal Compression Using Beta Wavelets. *Journal of Mathematical Modelling and Algorithms*, *11*(3), 235–248. https://doi.org/10.1007/s10852-012-9181-9

Kummer, K., Dummel, S., Bode, S. & Stahl, J. (2020). The gamma model analysis (GMA): Introducing a novel scoring method for the shape of components of the event-related potential. *Journal of neuroscience methods*, *335*, 108622. https://doi.org/10.1016/j.jneumeth.2020.108622

Lagarias, J. C., Reeds, J. A., Wright, M. H. & Wright, P. E. (1998). Convergence Properties of the Nelder--Mead Simplex Method in Low Dimensions. *SIAM Journal on Optimization*, *9*(1), 112–147. https://doi.org/10.1137/S1052623496303470

Lewis, R. M., Torczon, V. & Trosset, M. W. (2000). Direct search methods: then and now // Direct search methods: Then and now. *Journal of Computational and Applied Mathematics*, *124*(1-2), 191–207. https://doi.org/10.1016/S0377-0427(00)00423-4

Lopes da Silva, F. (1991). Neural mechanisms underlying brain waves: From neural membranes to networks. *Electroencephalography and Clinical Neurophysiology*, *79*(2), 81–93. https://doi.org/10.1016/0013-4694(91)90044-5

Luck, S. J. (2012). *Is it Legitimate to Compare Conditions with Different Numbers of Trials?* http://www.erpinfo.org/uploads/5/8/4/6/58469631/mean_peak_noise.pdf

Luck, S. J. (2014). *An introduction to the event-related potential technique* (Second edition). The MIT Press. http://site.ebrary.com/lib/alltitles/docDetail.action?docID=1088334

Makeig, S., Bell, A. J., Jung, T. P. & Sejnowski, T. J. (1996). Independent component analysis of electroencephalographic data. *Advances in Neural Information Processing Systems*(8), 145–151.

Masaki, H., Tanaka, H., Takasawa, N. & Yamazaki, K. (2001). Error-related brain potentials elicited by vocal errors. *Neuroreport*, *12*(9), 1851–1855.

Masaki, H. & Segalowitz, S. (2004). *Error negativity: A test of the response conflict versus error detection hypotheses.*

McGillem, C. D., Aunon, J. I. & Yu, K. B. (1985). Signals and noise in evoked brain potentials. *IEEE transactions on bio-medical engineering*, *32*(12), 1012–1016. https://doi.org/10.1109/TBME.1985.325510

Nelder, J. A. & Mead, R. (1965). A Simplex Method for Function Minimization. *The Computer Journal*, *7*(4), 308–313. https://doi.org/10.1093/comjnl/7.4.308

Neubauer, A. C. & Fink, A. (2009). Intelligence and neural efficiency. *Neuroscience & Biobehavioral Reviews*, *33*(7), 1004–1023. https://doi.org/10.1016/j.neubiorev.2009.04.001

Nieuwenhuis, S., Ridderinkhof, K. R., Blom, J., Band, G. P.H. & Kok, A. (2001). Error- related brain potentials are differentially related to awareness of response errors:

Evidence from an antisaccade task. *Psychophysiology*, *38*(5), 752–760. https://doi.org/10.1111/1469-8986.3850752

Nisar, H. & Kim, H. Y. (2015). Introduction to EEG and ERP Signals. In N. Kamel & A. S. Malik (Hg.), *EEG/ERP analysis: Methods and applications* (S. 2–21). CRC Press Taylor & Francis Group.

Nunez, P. L. & Srinivasan, R. (2006). *Electric fields of the brain: The neurophysics of EEG* (2. ed.). Oxford Univ. Press.

Oliveira, H. M. & Araújo, G.A.A. (2005). Compactly Supported One-cyclic Wavelets Derived from Beta Distributions. *Journal of Communication and Information Systems*, *20*(3), 105–111. https://doi.org/10.14209/jcis.2005.17

Ouyang, G., Herzmann, G., Zhou, C. & Sommer, W. (2011). Residue iteration decomposition (RIDE): A new method to separate ERP components on the basis of latency variability in single trials. *Psychophysiology*, *48*(12), 1631–1647. https://doi.org/10.1111/j.1469-8986.2011.01269.x

Perrin, F., Pernier, J., Bertrand, O. & Echallier, J. F. (1989). Spherical splines for scalp potential and current density mapping. *Electroencephalography and Clinical Neurophysiology*, *72*(2), 184–187. https://doi.org/10.1016/0013-4694(89)90180-6

Sagias, N. C. & Karagiannidis, G. K. (2005). Gaussian Class Multivariate Weibull Distributions: Theory and Applications in Fading Channels. *IEEE Transactions on Information Theory*, *51*(10), 3608–3619. https://doi.org/10.1109/TIT.2005.855598

Sanhueza, A., Leiva, V. & Balakrishnan, N. (2008). The Generalized Birnbaum– Saunders Distribution and Its Theory, Methodology, and Application. *Communications in Statistics - Theory and Methods*, *37*(5), 645–670. https://doi.org/10.1080/03610920701541174

Scheffers, M. K. & Coles, M. G. (2000). Performance monitoring in a confusing world: Error-related brain activity, judgments of response accuracy, and types of errors. *Journal of experimental psychology. Human perception and performance*, *26*(1), 141–151.

Scheffers, M. K., Coles, M. G., Bernstein, P., Gehring, W. J. & Donchin, E. (1996). Event-related brain potentials and error-related processing: an analysis of incorrect responses to go and no-go stimuli. *Psychophysiology*, *33*(1), 42–53. https://doi.org/10.1111/j.1469-8986.1996.tb02107.x

Šidák, Z. (1967). Rectangular Confidence Regions for the Means of Multivariate Normal Distributions. *Journal of the American Statistical Association*, *62*(318), 626–633. https://doi.org/10.1080/01621459.1967.10482935

Stahl, J. (2010). Error detection and the use of internal and external error indicators: an investigation of the first-indicator hypothesis. *International journal of psychophysiology : official journal of the International Organization of Psychophysiology*, *77*(1), 43–52. https://doi.org/10.1016/j.ijpsycho.2010.04.005

Stahl, J. & Gibbons, H. (2004). The application of jackknife-based onset detection of lateralized readiness potential in correlative approaches. *Psychophysiology*, *41*(6), 845–860. https://doi.org/10.1111/j.1469-8986.2004.00243.x

Stahl, J., Gibbons, H. & Miller, J. (2010). Modeling single-trial LRP waveforms using gamma functions. *Psychophysiology*, *47*(1), 43–56. https://doi.org/10.1111/j.1469- 8986.2009.00878.x

Tecce, J. J. (1972). Contingent negative variation (CNV) and psychological processes in man. *Psychological Bulletin*, *77*(2), 73–108. https://doi.org/10.1037/h0032177

Tenke, C. E. & Kayser, J. (2005). Reference-free quantification of EEG spectra: Combining current source density (CSD) and frequency principal components analysis (fPCA). *Clinical neurophysiology : official journal of the International Federation of Clinical Neurophysiology*, *116*(12), 2826–2846. https://doi.org/10.1016/j.clinph.2005.08.007

Thivierge, J.-P. (2007). Functional data analysis of cognitive events in EEG. In *IEEE International Conference on Systems, Man and Cybernetics, 2007: SMC 2007 ; 7 - 10 Oct. 2007, Montreal, QC, Canada* (S. 2473–2478). IEEE Service Center. https://doi.org/10.1109/ICSMC.2007.4413811

Tukey, J. W. (1977). *Exploratory data analysis*. *Addison-Wesley series in behavioral science : Quantitative methods*. Addison-Wesley.

Ulrich, R. (2009). Uncovering unobservable cognitive mechanisms: The contribution of mathematical models. In F. Rösler, C. Ranganath, B. Röder & R. Kluwe (Hg.), *Neuroimaging of Human MemoryLinking cognitive processes to neural systems* (S. 25–42). Oxford University Press. https://doi.org/10.1093/acprof:oso/9780199217298.003.0003

Ulrich, R. & Miller, J. (2001). Using the jackknife-based scoring method for measuring LRP onset effects in factorial designs. *Psychophysiology*, *38*(5), 816–827. https://doi.org/10.1017/S0048577201000610

Verleger, R. & Wascher, E. (1995). Fitting ex-Gauss functions to P3 waveshapes: an attempt at distinguishing between real and apaarent changes of P3 latency. *Journal of Psychophysiology*(9), 146–158.

Vidal, F., Burle, B., Bonnet, M., Grapperon, J. & Hasbroucq, T. (2003). Error negativity on correct trials: A reexamination of available data. *Biological Psychology*, *64*(3), 265–282. https://doi.org/10.1016/S0301-0511(03)00097-8

Vidal, F., Hasbroucq, T., Grapperon, J. & Bonnet, M. (2000). Is the 'error negativity' specific to errors? *Biological Psychology*, *51*(2-3), 109–128. https://doi.org/10.1016/S0301-0511(99)00032-0

Walter, W. G., Cooper, R., Aldridge, V. J., McCallum, W. C. & Winter, A. L. (1964). Contingent Negative Variation: An Electric Sign of Sensori-Motor Association and Expectancy in the Human Brain. *Nature*, *203*(4943), 380–384. https://doi.org/10.1038/203380a0

Weibull, W. (1951). A statistical distribution function of wide applicability. *J Appl Mech*(18), 290–293.

Woodman, G. F. (2010). A brief introduction to the use of event-related potentials in studies of perception and attention. *Attention, Perception & Psychophysics*, *72*(8), 2031–2046. https://doi.org/10.3758/APP.72.8.2031

Wright, M. H. (1996). Direct search methods: Once scorned, now respectable. *Pitman Research Notes in Mathematics Series*, 191–208.

Yeung, N., Bogacz, R., Holroyd, C. B., Nieuwenhuis, S. & Cohen, J. D. (2007). Theta phase resetting and the error-related negativity. *Psychophysiology*, *44*(1), 39–49. https://doi.org/10.1111/j.1469-8986.2006.00482.x

Yeung, N., Botvinick, M. M. & Cohen, J. D. (2004). The Neural Basis of Error Detection: Conflict Monitoring and the Error-Related Negativity. *Psychological Review*, *111*(4), 931–959. https://doi.org/10.1037/0033-295X.111.4.931

11 Appendix

Table A1. Study 1 - Mean and standard deviation (± *SD*) for the time-dependent and the shape-dependent gamma model parameters (first IP, mode, second IP, skewness, excess) for both simulated conditions and separately for simulated and estimated parameters and noise level (N=100).

Simulated Condition	*1*	*2*
Simulated Parameters		
First Inflection Point	52.63 ± 40.02	99.30 ± 37.78
Mode	97.89 ± 48.69	150.10 ± 44.95
Second Inflection Point	145.50 ± 57.47	202.97 ± 52.41
Skewness	0.45 ± 0.03	0.40 ± 0.02
Excess	0.31 ± 0.05	0.24 ± 0.03
Estimated Parameters		
Noise Level 1		
First Inflection Point	52.53 ± 40.12	99.36 ± 37.76
Mode	97.81 ± 48.68	150.02 ± 44.86
Second Inflection Point	145.44 ± 57.53	202.75 ± 52.25
Skewness	0.45 ± 0.03	0.40 ± 0.02
Excess	0.31 ± 0.05	0.24 ± 0.03
Noise Level 3		
First Inflection Point	52.89 ± 40.55	99.30 ± 38.09
Mode	97.96 ± 48.75	150.41 ± 46.03
Second Inflection Point	145.35 ± 57.22	203.64 ± 54.52
Skewness	0.45 ± 0.04	0.40 ± 0.03
Excess	0.31 ± 0.05	0.24 ± 0.03
Noise Level 6		
First Inflection Point	52.36 ± 40.26	97.48 ± 37.14
Mode	97.99 ± 48.43	149.03 ± 46.59
Second Inflection Point	146.05 ± 57.11	202.81 ± 57.34
Skewness	0.46 ± 0.04	0.40 ± 0.05
Excess	0.31 ± 0.05	0.25 ± 0.04

Table A2. Study 1 - *F*-value and *p*-value for the time-dependent and the shape-dependent estimated gamma model parameters (first IP, mode, second IP, skewness, excess) separately for the noise level (1 vs. 3 vs. 6) and simulated condition (1 vs. 2; N=100).

	F	*p*	η_p^2
Time-dependent parameters			
First Inflection Point			
Simulated Condition	71.46	<.01	.42
Noise Level	2.60	.08	.03
Noise Level by Simulated Condition	1.91	.15	.02
Mode			
Simulated Condition	62.37	<.01	.39
Noise Level	0.38	.68	<.01
Noise Level by Simulated Condition	0.55	.58	.01
Second Inflection Point			
Simulated Condition	55.05	<.01	.36
Noise Level	0.07	.93	<.01
Noise Level by Simulated Condition	0.25	.78	<.01
Shape-dependent parameters			
Skewness			
Simulated Condition	119.83	<.01	.55
Noise Level	2.21	.11	.02
Noise Level by Simulated Condition	0.35	.70	<.01
Excess			
Simulated Condition	126.98	<.01	.56
Noise Level	1.35	.26	.01
Noise Level by Simulated Condition	0.94	.39	.01

Table A3. Study 2 - Pearson's correlation coefficients, for the gamma model parameters (shape parameter, rate parameter, scaling, first IP, mode, second IP, skewness, excess) and classical ERP parameters (peak, area, latency) correlated with the reaction time (RT), time to peak (TTP) and the peak force (PF), separately for Response Type (error vs. correct; N=113). Corrected for multiple comparisons through Šidák correction.

	Error			**Correct**		
	median RT	**PF**	**TTP**	**median RT**	**PF**	**TTP**
GaM parameter						
Shape parameter	-.01	-.28	-.13	-.09	-.17	-.11
Rate parameter	<.01	-.32*	-.16	-.07	-.18	-.12
Scaling	.08	.20	.07	.04	.13	.12
1st IP	-.02	.03	-.08	-.17	<.01	-.04
Mode	-.08	.34*	.17	-.07	.10	.12
2nd IP	-.08	.34*	.20	<.01	.12	.16
Skewness	-.04	.34*	.29*	.12	.13	.17
Excess	-.05	.32*	.30*	.11	.11	.18
Classical Parameters						
Peak	-.23	.03	.11	-.02	-.06	.02
Area	.12	.11	<.01	.02	.15	.07
Latency	-.05	.36*	.20	-.07	.27	.25

*$p < .0008$

Table A4. Study 2 - Pearson's correlation coefficients, for the gamma model parameters (shape parameter, rate parameter, scaling, first IP, mode, second IP, skewness, excess) with classical ERP parameters (peak, area, latency), separately for Response Type (error vs. correct; N=113). Corrected for multiple comparisons through Šidák correction.

	Error			**Correct**		
	Peak	Area	Latency	Peak	Area	Latency
GaM parameter						
Shape parameter	.01	-.37*	-.27	.37*	-.52*	-.39*
Rate parameter	.02	-.41*	-.43*	.37*	-.51*	-.47*
Scaling	-.74*	.85*	.29	-.81*	.91*	.44*
1st IP	-.06	.02	.60*	.20	-.24	.16
Mode	.04	.13	.71*	<.01	.13	.59*
2nd IP	.07	.12	.54*	-.09	.26	.60*
Skewness	.07	.23	.35*	-.27	.46*	.47*
Excess	.10	.14	.34*	-.22	.41*	.44*

*p <.001

Table A5. Study 3 - Pearson's correlation coefficients, for the gamma model parameters (shape parameter, rate parameter, scaling, first IP, mode, second IP, skewness, excess) with classical ERP parameters (peak, area, latency), separately for Force Type (low PF vs. high PF) and TTP Type (short TTP vs. long TTP; N=18). Corrected for multiple comparisons through Šidák correction.

	Peak	**Area**	**Area**	**Latency**
Low PF – Short TTP				
1st IP	-.01	-.09	.28	.60
Mode	-.10	.20	-.56	.85*
2nd IP	-.07	.23	-.72	.59
Skewness	-.18	.36	-.75*	.16
Excess	-.08	.26	-.74*	.20
Low PF – Long TTP				
1st IP	.20	-.19	.01	.76*
Mode	.19	-.09	-.73*	.30
2nd IP	.18	-.08	-.91*	.21
Skewness	-.22	.38	-.74*	.17
Excess	-.10	.26	-.77*	.22
High PF – Short TTP				
1st IP	.22	-.23	-.19	.70*
Mode	.25	-.17	-.72	.70*
2nd IP	.20	-.11	-.71	.49
Skewness	-.05	.17	-.61	.17
Excess	.04	.06	-.59	.06
High PF – Long TTP				
1st IP	.40	-.54	-.21	.83*
Mode	.38	-.29	-.79*	.17
2nd IP	.34	-.24	-.81*	.06
Skewness	-.10	.30	-.68	-.23
Excess	-.07	.11	-.61	-.09

*p<.0006

Danksagung

Ein besonderer Dank gebührt den beiden wichtigsten Frauen in meinem Leben: meiner Tochter Tilda und meiner Frau Mareike – ohne euch wäre meine Leben nur halb so schön, aufregend und lebenswert.
Weiter möchte ich meiner Erstbetreuerin Frau Prof.'in Jutta Stahl danken, welche mir immer mit Rat und Tat zur Seite gestanden hat.
Vielen Dank auch an meine beiden Korrekturleser Dr. Paul Hüsing und André Mattes und nicht zu vergessen, der gesamte Lehrstuhl der Differentiellen Psychologie und Psychologische Diagnostik.
Ohne all die aufgezählten Personen hier wäre diese Dissertation in der vorliegenden Form nicht möglich gewesen – nochmals vielen Dank dafür!